



Title	Broadband cavity-enhanced absorption spectroscopy with incoherent light
Author(s)	Ruth, Albert A.; Dixneuf, Sophie; Raghunandan, R.
Editor(s)	Gagliardi, Gianluca Loock, Hans-Peter
Publication date	2014
Original citation	RUTH, A. A., DIXNEUF, S. & RAGHUNANDAN, R. 2014. Broadband Cavity-Enhanced Absorption Spectroscopy with Incoherent Light. In: GAGLIARDI, G. & LOOCK, H.-P. (eds.) Cavity-Enhanced Spectroscopy and Sensing. Berlin; Heidelberg: Springer Berlin Heidelberg. DOI: 10.1007/978-3-642-40003-2_14
Type of publication	Book chapter
Link to publisher's version	http://link.springer.com/chapter/10.1007/978-3-642-40003-2_14# http://dx.doi.org/10.1007/978-3-642-40003-2 Access to the full text of the published version may require a subscription.
Rights	© 2014, Springer-Verlag Berlin Heidelberg. The final publication is available at Springer via http://dx.doi.org/10.1007/978-3-642-40003-2_14
Embargo information	Access to this article is restricted until 12 months after publication by the request of the publisher.
Item downloaded from	http://hdl.handle.net/10468/1768

Downloaded on 2017-02-12T13:12:27Z



UCC

University College Cork, Ireland
Coláiste na hOllscoile Corcaigh

Broadband Cavity-Enhanced Absorption Spectroscopy with Incoherent Light

A. A. Ruth, S. Dixneuf, R. Raghunandan

Table of Contents

1	1. Introduction	2
2	2. Broadband cavity-based absorption spectroscopy.....	3
3	2.1 Classification of experimental broadband approaches	3
4	2.2 Time-dependent broadband methods.....	4
5	2.2.1 Cavity ring-down spectroscopy (CRDS).....	4
6	2.2.2 Phase-shift CRD spectroscopy.....	5
7	2.3 Intensity-dependent broadband methods	5
8	2.3.1 Measurement principles of IBBCEAS	6
9	2.3.2 Advantages and drawbacks of broadband CEAS	7
10	3. Experimental aspects	8
11	3.1 Light source considerations	8
12	3.2 Cavity considerations	12
13	3.2.1 Types of cavity used for BBCEAS with incoherent light sources	12
14	3.2.2 Linear cavity: open-path versus closed-path for <i>in situ</i> trace gas monitoring.....	16
15	3.2.3 Determination of mirror reflectivity	17
16	3.3 Detection schemes.....	19
17	3.3.1 Dispersive wavelength selection approaches	19
18	3.3.2 Interferometric wavelength selection approaches.....	20
19	3.3.3 Detection limit	22
20	4. Summary of literature.....	24
21	References	26

28

29

1. Introduction

Since the initial development of cavity ring-down spectroscopy (CRDS) in the late 1980s, the application of temporally and spatially incoherent light sources in cavity-enhanced spectroscopy has long been considered rather inappropriate, if not impossible. The reason for this perception was due to the generally significantly lower brightness of incoherent light sources (in comparison to lasers), and their low coupling efficiency to high finesse optical cavities [1]. At first glance, these apparently adverse features make cavity-enhanced absorption spectroscopy (CEAS) with incoherent light appear unattractive. However, there is also a multitude of advantages of using incoherent broadband light for CEAS that have motivated a significant number of experimental implementations in analytical and spectroscopic applications.

Experimentally all broadband CEAS methods^{#1} have in common that wavelength selection takes place after the cavity. This removes the need for scanning the wavelength and introduces the possibility of multiplexed light detection. Even though the coupling efficiency for truly white light^{#2} to high finesse cavities is rather low, at any given time, incoherent light (or spectrally broad light of limited temporal coherence) contains frequencies that correspond to the eigen-modes of a cavity for a given geometry, i.e. for a certain cavity length, mirror radius of curvature and diameter. Therefore a certain fraction of the light will always couple to the cavity. In a typical experiment white light entering the cavity, both on- and off-axis, will excite all accessible axial and transverse modes of the cavity for the given excitation conditions. As the mirrors are subject to small fluctuations (e.g. vibrations or minor mechanical instabilities) and slow thermal drift, the cavity modes are moreover continuously modified. Since the **superposition principle** holds inside the cavity [3], the transmitted light will not exhibit a mode structure (or mode effects), as observed in case of coherent excitation of cavities with narrow band lasers. The mode structure of the cavity plays no role in the measurement principle, which is solely based on the increase of the absorption path length by the cavity. The spectral resolution of broadband CEAS thus depends only on the approach chosen to select a wavelength of the light transmitted through the cavity.

The various experimental implementations of broadband cavity-enhanced absorption methods have been the subject of several reviews [4,5]. Generally one can distinguish between methods that determine the characteristic photon storage time in the cavity (ring-down approach [6] or phase shift measurements [7]), and methods that measure the light intensity transmitted through the cavity [8]. This book chapter predominantly aims at the discussion of the latter type of approach. In section 2 the general principles of **broadband CEAS** are outlined and general 'pros and cons' discussed. Section 3 outlines different aspects concerning light sources, cavity considerations and detection schemes. In section 4, a comprehensive overview of the current literature based on a methodological classification scheme is presented.

^{#1} The principle of measuring the cavity transmission directly to determine the loss inside a cavity was first implemented by O'Keefe [2] who used a **pulsed** cavity ring-down setup and named the approach "integrated cavity output spectroscopy" (ICOS). Besides CEAS as an acronym for **cw** applications, the abbreviation ICOS is also found in the literature.

^{#2} The term "white light" will be used synonymously for "incoherent broadband over a certain spectral region".

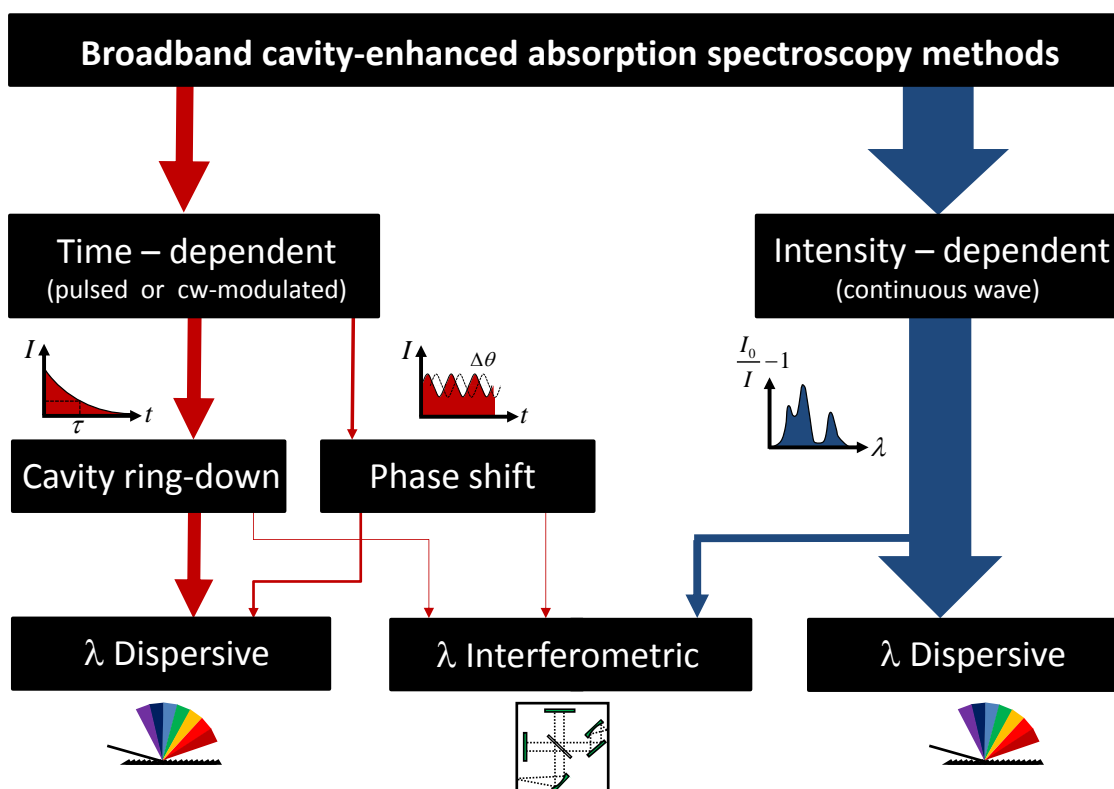
2. Broadband cavity-based absorption spectroscopy

2.1 Classification of experimental broadband approaches

Figure 2.1 gives a general overview of broadband cavity-enhanced absorption methods, which can be broadly divided into two categories.

(A) *Time-dependent methods* are based on the measurement of the time that light can be stored inside the cavity (referred to as cavity ring-down spectroscopy, CRDS – section 2.2). The excitation light source is generally pulsed (or cw-modulated).

(B) *Intensity-dependent methods* are based on the measurement of the broadband light transmitted through the cavity (referred to as cavity-enhanced absorption spectroscopy, CEAS – section 2.3). The excitation light source is commonly continuous wave.



11
12

13 **Figure 2.1:** Classification of broadband cavity-enhanced absorption approaches and detec-
14 tion schemes. The widths of the arrows indicate the relative number of occurrences of the
15 type of approach in the literature.

16

17 All approaches use experimental multiplexing features to establish a wavelength-dependent
18 optical loss spectrum "in one go". The time resolution in most applications can be very high,
19 but depends ultimately on the detection scheme and spectral resolution. The basic measure-
20 ment principles are briefly outlined in this section followed by a discussion of several advan-
21 tages and drawbacks of specific approaches/properties for certain applications.

2.2 Time-dependent broadband methods

2.2.1 Cavity ring-down spectroscopy (CRDS)

The intensity, I , of broadband light in a cavity after pulsed injection decays exponentially according to the wavelength-dependent mirror reflectivity, $R(\lambda)$,^{#3} and losses, $L(\lambda)$, associated with the optical extinction (absorption and scattering) of the sample inside the cavity [9]:

$$I(t, \lambda) = I_{t=0} \exp\left(-\left[(1-R(\lambda)) + L\right] \frac{tc}{d}\right), \quad (1)$$

where d is the length of the cavity and c is the speed of light. The time it takes the light intensity to reduce to e^{-1} of its initial value, $I_{t=0}$, is known as the ring-down time (see T. Miller et al. in this book):

$$\tau(\lambda) = \frac{d}{c\left[(1-R(\lambda)) + L(\lambda)\right]}. \quad (2)$$

For an empty cavity, the ring-down time is given by $\tau_0 = d/[c(1-R)]$ and hence the optical loss can be calculated as

$$L(\lambda) = \frac{d}{c} \left(\frac{1}{\tau(\lambda)} - \frac{1}{\tau_0(\lambda)} \right). \quad (3)$$

The loss L depends on the sample in the cavity and/or the way it has been prepared. In most cases L is in good approximation a Lambert-Beer loss and can be described as $L = \varepsilon d'$, where ε is the extinction coefficient of the sample containing contributions from absorption and scattering, and $d' \leq d$ is the physical length of the sample inside the cavity.

The difference between broadband and conventional CRD spectroscopy is that broadband approaches measure multiple ring-down events as a function of wavelength simultaneously and hence possess multiplexing character. Wavelength selection and detector electronics typically require a time resolution of less than one μs to capture ring-down events [4]. As an example, a fast-rotating mirror in conjunction with a diffraction grating was used by Scherer et al. [10] to record the time and wavelength response of an optical cavity along orthogonal axes (time along the vertical axis, wavelength along the horizontal axis) of a CCD array detector. Wavelength-dependent ring-down times are acquired for each independent decay event. In another experimental implementation by Ball et al. [6] a two dimensional clocked CCD array was used at the exit of a spectrograph dispersing the light exiting the cavity. By applying suitably phased voltages to the electrodes along one of the axes of the pixel array, charge can be transferred efficiently between rows of CCD pixels in either direction. This enables a clocking sequence for images to be transferred between vertical pixels, permitting the continuous two dimensional acquisition of ring-down events [5,11]. The technique has been applied to atmospheric field studies for ambient concentration measurements of I_2 , OIO , NO_2 , NO_3 , N_2O_5 [12-14]. More recent variants of broadband CRDS have seen the combination of the technique with white light supercontinuum sources [15-18].

^{#3} $R(\lambda) = \sqrt{R_1 R_2}$, where R_1, R_2 are the reflectivities of the individual cavity mirrors (Figure 2.2).

1 2.2.2 Phase-shift CRD spectroscopy

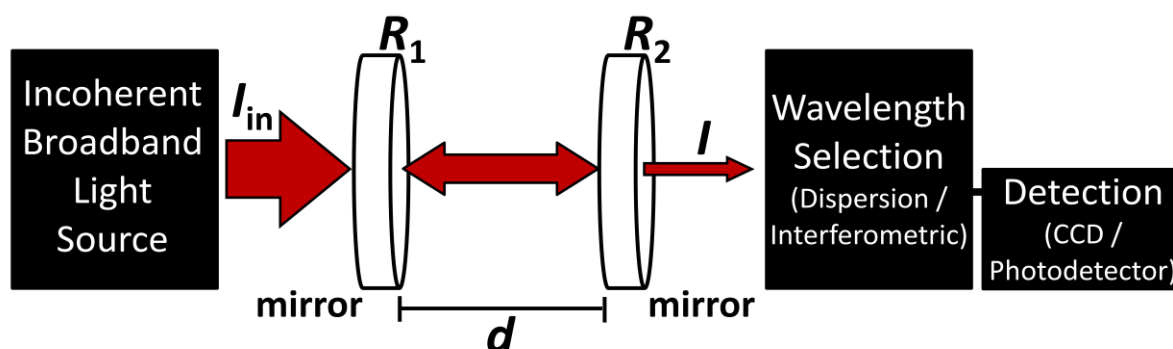
2 In phase shift CRDS [19,20], intensity modulated narrow band light (from a cw laser) is in-
3 jected into a high finesse cavity. Due to the delay introduced by the optical cavity, the modu-
4 lation on the light exiting the cavity is shifted in phase by $\phi(\lambda)$, which is related to the ring-
5 down time, $\tau(\lambda)$, and the angular modulation frequency, Ω , by:

$$6 \quad \tau(\lambda) = -\Omega^{-1} \tan [\phi(\lambda)]. \quad (4)$$

7 Thus absorption information is deduced from the wavelength-dependent phase shift that the
8 modulated beam undergoes upon passing through the cavity. In the broadband version by
9 Hamers et al. [7] the intensity-modulated light of a high pressure cw xenon arc was directed
10 into the cavity after passing through a Fourier Transform (FT) spectrometer, and the light
11 transmitted through the cavity was detected by a photomultiplier tube. The ratio of the FT of
12 the in-phase and out-of-phase components of the intensity modulated light exiting the cavity
13 (determined with a lock-in amplifier) gave the absorption information of the sample. This al-
14 lowed highly sensitive absorption measurements of the spin forbidden $b(0,0) \leftarrow X$ transition
15 (A-band) of molecular oxygen in air, at a resolution determined by the interferometer over
16 250 nm.

17 2.3 Intensity-dependent broadband methods

18
19 In CEAS with incoherent broadband (IBB) light sources, the time-integrated steady-state
20 light intensity transmitted through the cavity is measured, which is inversely proportional to
21 the extinction coefficient, ε . The use of incoherent light sources was first experimentally
22 demonstrated with a short-arc Xe lamp in 2003 [8] by measuring the forbidden $b(2,0) \leftarrow X$
23 transition (γ -band) of O_2 and the $S_1 \leftarrow S_0$ absorption of gaseous azulene. Figure 2.2 shows a
24 basic schematic of the implementation of an IBBCEAS setup.



25
26 **Figure 2.2:** Schematic of the experimental implementation of incoherent broadband cavity-
27 enhanced absorption spectroscopy (IBBCEAS). The cavity is formed by two highly reflective
28 spherical mirrors of reflectivity R_1 and R_2 which are separated by a distance d . Intensities of
29 light incident on and transmitted through the cavity are denoted I_{in} and I , respectively. Note:
30 $R = (R_1 R_2)^{0.5}$

31
32 The spectral resolution of IBBCEAS depends solely on the way the wavelength of the trans-
33 mitted light is selected. Dispersive methods (typically grating spectrographs with multichan-

1 nel detectors) enable high time resolution but limited selectivity, while interferometric ap-
 2 proaches permit a high spectral resolution but a limited time resolution (see section 3.3).

3 2.3.1 Measurement principles of IBBCEAS

4 Consider a cavity of length d formed by two mirrors of reflectivity $R(\lambda)$ which is continu-
 5 ously excited with incoherent light of intensity I_{in} (see Figure 2.2). Irrespective of the cavity's
 6 mode structure (see introduction) the intensity of light transmitted through the cavity, I , cor-
 7 responds to the sum of photons leaking out of the cavity after an odd number of passes. For a
 8 cavity containing a sample with losses, $L(\lambda)$, this **superposition** of light transmitted through
 9 the cavity can be represented by the geometric series:

$$11 \quad I = I_{in} (1-R)^2 (1-L) \sum_{n=0}^{\infty} (1-L)^{2n}. \quad (5)$$

12 For eq. (5) to hold, the transmission integration time t is assumed to be substantially larger
 13 than the ring-down time, τ . Since $R < 1$ and $L < 1$ this series converges to:

$$15 \quad I = I_{in} \frac{(1-R)^2 (1-L)}{1-R^2(1-L)^2}. \quad (6)$$

16 For a resonator without sample losses ($L = 0$) eq. (6) simplifies to:

$$17 \quad I_0 = I_{in} \frac{1-R}{1+R}. \quad (7)$$

18 Provided that the attenuation of light per pass is caused by Lambert-Beer losses, i.e.
 19 $(1-L(\lambda)) = \exp(-\varepsilon(\lambda)d)$, the **extinction coefficient**, ε can be written as:

$$21 \quad \varepsilon(\lambda) = \frac{1}{d} \ln \left[\frac{1}{2R^2(\lambda)} \left(\sqrt{4R^2(\lambda) + \left(\frac{I_0(\lambda)}{I(\lambda)} (R^2(\lambda) - 1) \right)^2} + \frac{I_0(\lambda)}{I(\lambda)} (R^2(\lambda) - 1) \right) \right], \quad (8)$$

22 irrespective of the magnitude of the loss per pass, εd . Note that the mirror separation d must
 23 be replaced by the physical length of the sample inside the cavity, $d' \leq d$, if the sample does
 24 not fill the entire cavity (see section 2.2). In case of small losses per pass ($L \rightarrow 0$) and high
 25 reflectivities of the mirrors ($R \rightarrow 1$), ε can be approximated by:

$$26 \quad \varepsilon(\lambda) \approx \frac{1}{d} \left(\frac{I_0(\lambda)}{I(\lambda)} - 1 \right) (1-R(\lambda)). \quad (9)$$

27 Eq. (9) demonstrates that the effective **path length** in IBBCEAS is increased by a factor of $(1$
 28 $- R)^{-1}$ in comparison to a single pass. The signal-to-noise ratio, however, is only improved by
 29 a factor of $[2(1-R)]^{-1/2}$ assuming a photon-noise limited experiment and negligible absorp-
 30 tion losses in the mirrors [21]. Fiedler et al. have studied in detail the influence of cavity pa-
 31 rameters like the cavity length, mirror curvature and reflectivity, different light injection ge-
 32 ometries on the IBBCEAS signal [22].

33 As opposed to time-dependent approaches where the mirror **reflectivity** can be deter-
 34 mined through measurements with an empty cavity, R needs to be calibrated in case of inten-

1 sity-dependent methods for the measurement of absolute extinction coefficients. A number of
2 ways to determine $R(\lambda)$ will be given in section 3.3.

3 **2.3.2 Advantages and drawbacks of broadband CEAS**

4 In order to get an overview of the benefits and weaknesses involved, the general properties of
5 broadband cavity-enhanced absorption methods with incoherent light sources will be outlined
6 in the context of the commonly desirable attributes of spectroscopic absorption methods:
7

8 **(1) Sensitivity:** A key criterion for the quality of an absorption technique is the smallest possible
9 detection limit for one or more target species. The detection limit is essentially based on
10 the effective absorption path length over which the light can interact with a sample for a
11 given signal-to-noise ratio, which depends on a given integration time and long-term stability
12 of the experimental setup (see section 3.3.3). As a result of the low photon flux and coupling
13 efficiency of incoherent light, ultimate sensitivities, as they can be achieved by mode match-
14 ing a narrow band laser to the modes of a high finesse cavity, cannot be reached. However,
15 3σ minimum detectable extinction coefficients of $2.4 \times 10^{-9} \text{ cm}^{-1} \text{ Hz}^{-1/2}$ have been reported
16 [23].

17 The sensitive detection of species can be done on an absolute (quantitative) or on a relative
18 scale. Absolute extinction measurements require the rigorous calibration of the mirror reflect-
19 ivity (section 3.2.3), which is especially critical in broadband techniques where the high re-
20 flectivity of low loss mirrors can exhibit significant wavelength-dependent variations depend-
21 ing on the spectral bandwidth of the mirrors.

22 In contrast to ring-down approaches, there is in principle no constraint on the upper limit of
23 the dynamical range over which incoherent broadband CEAS methods are applicable [8]. A
24 practical limit is reached when optical losses can be measured in a single pass. That makes
25 broadband methods attractive to systems that exhibit inherent losses such as transparent liq-
26 uids or solids (see item **(5)** below).

27 **(2) Selectivity and multi-component detection:** The selectivity of an instrument is its ability
28 to distinguish between different species absorbing at similar wavelengths; it depends on the
29 thermodynamic state of the sample and the way it has been prepared. Although many differ-
30 ent species may absorb light at one or more wavelengths, the total spectral profile of any par-
31 ticular species is unique. In practice, the high reflectivity range of the cavity mirrors and the
32 spectral characteristics of light sources always limit the wavelength range available to probe a
33 given sample. As a result, selecting an appropriate wavelength range that is specific to the
34 target species can pose a serious challenge, especially if sample mixtures (i.e. "interfering"
35 species) are present or several loss processes dominate the experiment. If an absorption
36 method is not combined with another non-spectroscopic analytical approach to separate sam-
37 ple species (e.g. chromatographic techniques, filtering, titration, mass selection by ionization,
38 to name a few), the spectral resolution is generally a measure for the method's capability to
39 distinguish between different species.

40 Broadband methods allow a significant spectral range to be covered simultaneously. This
41 multiplex advantage enables several species to be monitored at once, while gathering infor-
42 mation over the entire spectral region. While dispersive methods (typically grating spectro-
43 graph with multichannel detectors) enable high time resolution (hence short integration
44 times) but limited selectivity, interferometric approaches permit a high spectral resolution but
45 a limited time resolution.

1 **(3) Time resolution:** An ideal spectroscopic absorption approach should achieve a "high"
2 sensitivity with a high time resolution (i.e. short integration times) to enable the study of dy-
3 namics, e.g. reaction kinetics, molecular processes or flow dynamics. Obviously sensitivity
4 and time resolution are connected via the achievable signal-to-noise ratio and hence the de-
5 tection limit. In case of an interferometric detection scheme the required spectral resolution
6 also affects the time resolution. Integration times from the ms range [24,25] (condensed
7 phase) to many hours [26] (high resolution FT experiment) have been reported in the litera-
8 ture. A natural lower limit of the time resolution for cavity-enhanced methods is the ring-
9 down time. For integration times that are shorter than the ring-down time, eq. (5) does not
10 hold anymore. If the system's dynamics proceeds on a time scale on the order of or smaller
11 than the ring-down time, the analysis procedure outlined in section 2.3.1 will become time-
12 dependent and the geometric series in eq. (5) becomes a time-dependent integral.

13 **(4) Versatility / Adaptability:** Since absorption spectroscopy is a universal tool in atomic
14 and molecular sciences, ideally an absorption method should be applicable to gaseous, liquid,
15 or solid systems and the corresponding interfaces. The principle applicability of a method
16 over a wide spectral range is a criterion for its versatility. Depending on the light source and
17 the high reflectivity range of the mirrors, broadband CEAS methods offer a high degree of
18 adaptability. Even though cavity-enhanced methods have been primarily developed for gas
19 phase absorption measurements, the absorption enhancement principle by increasing the in-
20 teraction path length with the sample is, of course, also applicable for liquid phase systems,
21 transparent solids, films and surface layers on substrates and internal reflection optics [Loock
22 et al. in this book,21,24,27-31].

23 Generally, the higher the mirrors' reflectivity (i.e. the higher the method's sensitivity), the
24 smaller is the usable wavelength range and hence the versatility of the approach. An experi-
25 mental approach to overcome these restrictions is outlined in section 3.2.1.

26 **(5) Practical parameters:** Other aspects that constitute practical advantages of sensitive de-
27 tection methods relate to the experimental approach being (a) compact or even potentially
28 portable, (b) uncomplicated to implement and "user-friendly", (c) robust and stable/durable,
29 (d) inexpensive with low maintenance requirements. Some of the broadband approaches
30 summarized in section 4 possess several of these advantages. The sensitivity to optical align-
31 ment, complexity, size or cost of some cavity-enhanced absorption methods and also that of
32 outright different techniques, such as degenerate four wave mixing, photoacoustic spectro-
33 scopy, resonance enhanced multi-photon ionization spectroscopy, or intracavity laser absorp-
34 tion spectroscopy, deter their widespread adoption for field observations or common applica-
35 tion in commercial analytical laboratories.

36 **3. Experimental aspects**

37 **3.1 Light source considerations**

38
39 The choice of light source (pulsed, modulated or continuous wave) essentially determines the
40 type of experimental broadband scheme (cf. Figure 2.1) and also governs the signal-to-noise
41 ratio for a given detection system. The favourable attributes of light sources listed below un-
42 der **(a)...**(d) should be considered for a successful implementation of the benefits of broad-

1 band cavity-enhanced setups, as discussed in section 2.3.2:

2
3
4 **(a)** *Broad unstructured emission spectrum*: For light sources whose emission bandwidth
5 is broader than the high reflectivity range of the cavity mirrors, rigorous filtering of wave-
6 lengths outside the high reflectivity range is essential in order to suppress the detection of
7 unwanted stray light. Very broad emission spectra provide a high degree of flexibility in
8 terms of switching between different excitation ranges, without major alterations on the exci-
9 tation side of the experiment. If the emission spectrum is smooth and unstructured, then spec-
10 tral intensity fluctuations that are inherent to the source have less negative effects on cavity
11 absorption measurements (see **(d)**).

12 **(b)** *High spectral brightness*: The number of photons incident on the cavity per unit area
13 and time ought to be as large as possible because of the unfavourable coupling efficiency of
14 broadband (temporally incoherent) light to high finesse cavities. The smaller the emitting
15 area for a specific output power (i.e. the higher the spatial coherence at the source's exit aper-
16 ture) the better are the imaging properties of the source. However, increasing spatial coher-
17 ence through spatial filtering is accompanied by a reduction in intensity [W m^{-2}]. The key
18 quantity that should therefore be maximized for broadband cavity-enhanced applications is
19 the spectral radiance [$\text{W m}^{-2} \text{sr}^{-1} \text{nm}^{-1}$].

20 **(c)** *High emission stability and low spectral noise/drift*: For (intensity-dependent) abso-
21 lute extinction measurements the spatial and spectral stability of the light source is of great
22 importance. (Narrow) line features in the emission spectrum or significant spectral intensity
23 gradients can be difficult to account for by reference measurements (without sample) even if
24 the light source exhibits only small intensity fluctuations. Attention should be paid to not
25 commence measurements during warm-up of the light source, when potential spectral drifts
26 and output intensity changes are very common.

27 **(d)** *Robustness, compactness, low maintenance, low cost, long lifetime*: Some of these
28 very practical attributes of light sources constitute key advantages of broadband CEAS and
29 may well determine the choice of light source for a specific application as well as outweigh
30 some of the experimentally important features (a) to (c). Preference for one of the attributes
31 (a) to (c) at the expense of another is often given based on the aspects listed under (d).

32 The following section summarizes the most important properties of light sources commonly
33 used in broadband CEAS (the list is exclusive of frequency comb sources – Maslowski & Ye;
34 Bernhardt et al. in this book).

35 36 **Arc lamps**

37 Corresponding to the colour temperature (typically several thousand K) arc lamps produce a
38 white light continuum that can cover the spectral region from the onset of the vacuum UV to
39 the near IR [32]. For Xe arcs atomic lines contribute mainly in the region between 750 and
40 1000 nm to the total optical power and to a lesser extent around 475 nm, leaving the remain-
41 der of the visible output rather insensitive to line fluctuations. Since generally the size of the
42 plasma arc scales with the wattage rating of the bulb, higher power lamps are not necessarily
43 more appropriate for broadband cavity applications. On the contrary, light emerging from an
44 extended area cannot be imaged as well as the light from a small (quasi point) source. While
45 most Xe-arc lamps have a *diffuse* arc where the area of light emission is distributed across the

1 entire plasma, Varma et al. [33] used a short-arc Xe lamp with a *hot spot*, where ca. 80% of
2 the emission come from a plasma spot of the dimensions of 150 μm yielding a spectral radi-
3 ance of $18 \text{ W cm}^{-2} \text{ sr}^{-1} \text{ nm}^{-1}$ at 400 nm [34]. However, the arc is prone to erratic jumps and
4 wandering of the hot spot, which requires an active spot stabilization.

5 For high resolution applications requiring Fourier transform detection (see section 3.3.2),
6 *superquiet* current stabilized Xe lamps (type Hamamatsu) with typical intensity fluctuations
7 of 0.2% and drifts of $\pm 0.5\%/h$ are useful, because longer integration times are generally re-
8 quired and unwanted high frequency noise introduced by arc movement is to be avoided to
9 maximize the signal-to-noise ratio [35].

10 For many years Xe-arc lamps have been the "work horse" for spectroscopic techniques such
11 as long-path differential optical absorption spectroscopy (LP-DOAS) [36]. In the context of
12 cavity-enhanced absorption spectroscopy they have been first applied in 2003 [8]. There have
13 been numerous applications in incoherent broadband cavity-enhanced absorption spectroscopy
14 (IBBCEAS) [8,21,26,35,37-44], but also broadband phase-shift CRD spectroscopy
15 (PSCRDS), where the intensity of the light needs to be modulated before entering the cavity
16 [7]. Furthermore, Walsh and Linnartz showed recently that the plasma emission in a super-
17 sonic jet can also be used to enhance the observability of self-absorption in the plasma [45].

18 19 **Halogen lamps**

20 Halogen lamps emit a smooth continuous spectrum from the near UV to the near IR. Their
21 advantage over Xe lamps is the absence of emission lines and price. However, their inferior
22 brightness and the large size of the emitting filament make them less suitable for broadband
23 CEAS. Their main application is in absorption systems with inherently large losses occurring
24 for instance in condensed phase studies [21,25,46].

25 26 **Light emitting diodes (LED)**

27 High power *LEDs* are power efficient, compact, generally inexpensive and long lived (up to
28 $>10000 \text{ h}$).

29 *Coloured LEDs* which are sufficiently bright for CEAS are now available in spectral
30 windows from the near infrared to the near UV ($> 350 \text{ nm}$). Being sensitive to temperature
31 fluctuations they are prone to (thermal) spectral drifts and hence require adequate temperature
32 and current stabilization for cavity applications. LED spectra typically shift towards longer
33 wavelengths when the temperature increases [47]; slight tuning of the wavelength range can
34 be achieved in that way to adapt the output spectrum to the reflectivity range of the mirrors
35 [48]. E.g. based on a temperature stabilization of $\pm 1 \text{ mK}$, Ventrillard et al. [49] reported that
36 the spectral drift of the emission spectrum of their red LED (625 nm) was smaller than 0.015
37 nm, while the total intensity fluctuation was better than 0.02% per hour. When stabilized ap-
38 propriately, LEDs emit a rather smooth quasi-Gaussian [47] or Lorentzian [48] spectrum over
39 typically a few tens of nm (FWHM), although emission bandwidth can vary from manufac-
40 turer to manufacturer (up to 50 nm, [48]). Depending on the FWHM of the LED spectral fil-
41 tering is less stringent but still recommended.

42 *White LEDs* (e.g. based on the excitation of an emitting phosphor in the blue [31])
43 cover large parts of the visible spectrum simultaneously. Often LED arrays are used to
44 achieve high optical output powers. However, due to the larger overall surface area (typically
45 a few mm^2) the imaging properties of arrays are generally inferior.

1 The application of LEDs in IBBCEAS was first demonstrated by Ball et al. [48] in the green
2 (535 nm) and red (661 and 665 nm) parts of the visible spectrum. LED based IBBCEAS has
3 since been widely applied for gas phase spectroscopy in the visible [49-58] and in the near-
4 UV [59-61], but also for liquid phase spectroscopy [27,28,62]. LEDs have also been used in
5 conjunction with cavity attenuated phase shift (CAPS) spectroscopy [63,64].

6 **Superluminescent light emitting diode** (SLEDs) are based on the generation and am-
7 plification of spontaneous emission in a semiconductor waveguide over a broad wavelength
8 range. Their emission bandwidth can vary from 5 to 100 nm. SLEDs therefore combine beam
9 divergence and power density comparable to that of a single-mode laser diode with the low
10 temporal coherence of a conventional LED [65]. SLEDs have not been extensively used as
11 light sources for CEAS measurements yet (e.g. [66-68]) and some studies compare their per-
12 formance to that of supercontinuum sources (see below).

13 **Supercontinuum sources: ‘white fibre lasers’**

14 In supercontinuum (SC) sources a broad spectral emission is generated by pumping a certain
15 length of a highly non-linear micro-structured **photonic crystal fibre** (PCF) with short (fs up
16 to ns) pulses from a seed laser, generally using a high repetition rate (kHz to MHz) [69]. The
17 well collimated fibre output has a high power density (up to several mW per nm) and is spec-
18 trally very broad; it typically extends from the blue region of the spectrum (> 400 nm) to the
19 near-IR (<2.5 μm) for a pump wavelength around 1060 nm. Significant performance insta-
20 bilities can be caused by optical feedback into the PCF, making operation with an optical cav-
21 ity critical due to the strong back reflection from the entrance cavity mirror (especially when
22 working around the seed wavelength). SC sources are also prone to exhibit considerable
23 power as well as spectral fluctuations, which have adverse effects in cavity applications.

24 In 2008 the first applications of SC sources to broadband CEAS were reported. In the wave-
25 length range 630-700 nm Langridge et al. [23] used an SC source for NO_3 and NO_2 detection
26 and reported the stability of the transmission spectra to vary between 0.2 and 0.5 % over 100
27 consecutive (2 s) acquisitions. Other examples of application of SC sources are briefly out-
28 lined in section 3.2.1 and listed in section 4. A somewhat different approach to create contin-
29 uum radiation for broadband CRD spectrography was taken by Stelmaszczyk et al. [16], who
30 generated plasma filaments in quartz instead of using a PCF.

31 *Comparative Studies*

32
33 Van der Sneppen et al. [31] compared the performance of a 1 W white LED with an
34 emission spectrum from 420-650 nm to that of an SC source in the context of evanescent-
35 wave BBCEAS. In this specific comparison the measurements taken with the SC source were
36 reported to have much lower baseline noise (by an order of magnitude) and higher precision
37 (by a factor of ~ 1.7) [31]. Denzer et al. [67] compared the performance of two near-IR
38 SLEDs, whose outputs were combined using a polarizing beam-splitter, to that of an SC
39 source in the context of Fourier transform CEAS. The optical power from the SC source
40 (within the range 1600-1700 nm) was four times higher than the total optical power incident
41 on the cavity from the combined SLEDs. Using a FT spectrometer with a maximal spectral
42 resolution of 4 cm^{-1} a significant sensitivity improvement from a minimal detectable absorp-
43 tion of $2 \times 10^{-8} \text{ cm}^{-1}$ to $5 \times 10^{-9} \text{ cm}^{-1}$ in a 4 min acquisition time was observed upon swap-
44 ping the SLEDs for the SC source.
45

1 Generally, when SC sources are used in conjunction with high resolution Fourier-
2 transform detection, instabilities in the SC output or due to the presence of intrinsic etalon
3 effects can be observed, negatively affecting performance [66,70].
4

5 **Non mode-locked nanosecond broadband lasers**

6 Among the sources with high directionality, nanosecond dye lasers without dispersive optical
7 element have been commonly applied in pulsed broadband cavity applications [4,6,71,72].
8 They produce lasing and/or strong amplified spontaneous emission (ASE) over a bandwidth
9 which is determined by the laser dye (or dye mixture). Broadband dye lasers typically emit
10 light over tens of nanometer in the visible (or near UV or IR) and do not require rigorous
11 spectral filtering of wavelengths outside the high reflectivity range of the mirrors. Due to the
12 good spatial coherence and high power density of the emitted light the injection into a high
13 finesse cavity can be effective even without mode-matching. Since broadband dye lasers can
14 exhibit significant shot-to-shot fluctuations and spectral structure in the emission, they are not
15 particularly appropriate for applications depending on the cavity transmission [1]. While the
16 first application of a "broadband" nanosecond dye laser was in Fourier transform CRDS en-
17 abling simultaneous monitoring of a 400 cm^{-1} broad spectral range in the near-IR [73], most
18 applications have been in broadband CRDS [4,6,12,48], broadband ring-down spectral pho-
19 tography [10], and cavity-ring-down spectrography [71]. In the latter the tuning element and
20 the output mirror of the dye laser were removed, enabling suppression of commonly excited
21 high order transverse modes. A drawback of (expensive) dye lasers is that they are not partic-
22 ularly compact and only moderately flexible in term of quick and straightforward wavelength
23 range selection, which requires changing the dye.

24 *A short pulsed free-electron laser* running at high repetition rate (ca. 12 MHz), characterized
25 by very good beam quality and stability over a 25 nm FWHM, was used for broadband
26 (pulse-stacked) CRDS in the infrared [74].
27

28 **3.2 Cavity considerations**

29 **3.2.1 Types of cavity used for BBCEAS with incoherent light sources**

30 **Linear cavities**

31 By far the most common geometry is the conventional linear (two-) mirror cavity
32 (Figure 2.2). Fiedler et al. [22] studied the influence of various cavity parameters on the sig-
33 nal-to-noise ratio (SNR) for IBBCEAS. According to this study, a symmetric confocal linear
34 cavity with converging light injection produces the optimal SNR. The maximum SNR with a
35 symmetric near-confocal cavity configuration is easier to achieve for large mirror separations
36 than for short cavities. The optimum use of linear cavities requires the f number of the cavity
37 to be adapted to that of the spectrometer.
38

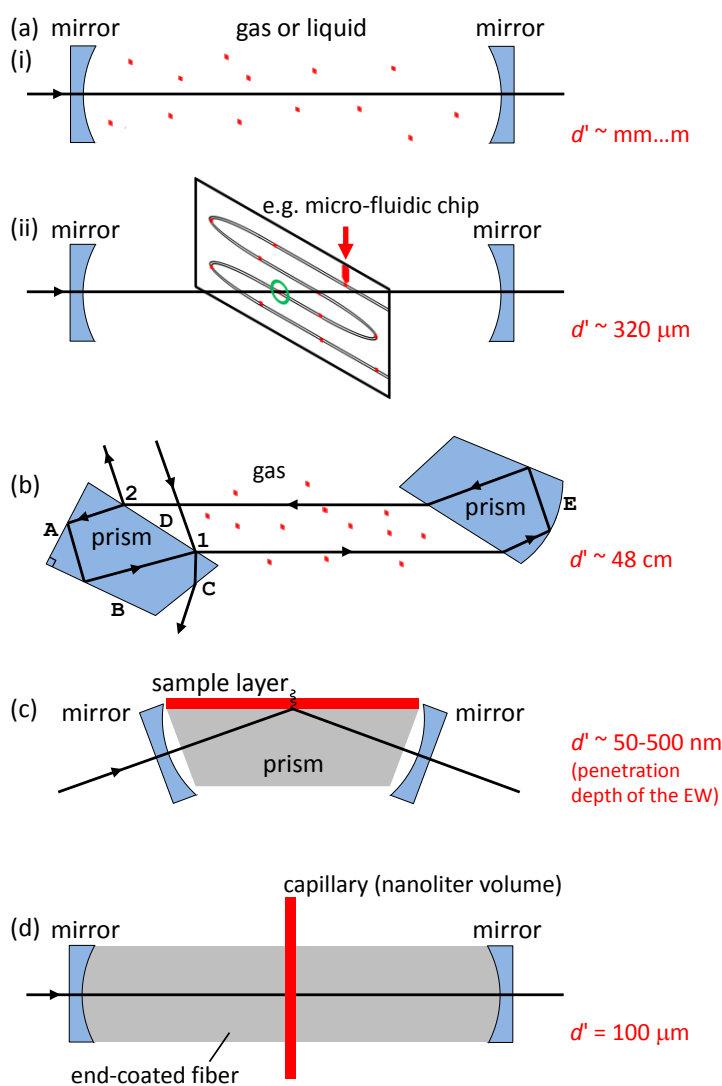
39 The large majority of studies carried out with linear (two-) mirror cavities focus on
40 the detection of **gas phase** species (see section 4), mostly employing setups where the cavity
41 is enclosed by a flow [38-40] or static cells [8,41,48] at high or modest pressures, or by vac-
42 uum chamber for low pressure regime [37,45,75]. In some atmospheric applications open-
43 path configurations were also used (Figure 3.1(a.i)), e.g. in conjunction with atmospheric
44 simulation chambers. Closed-path and open-path configurations present advantages and

1 drawbacks which will be discussed in detail in section 3.2.2.

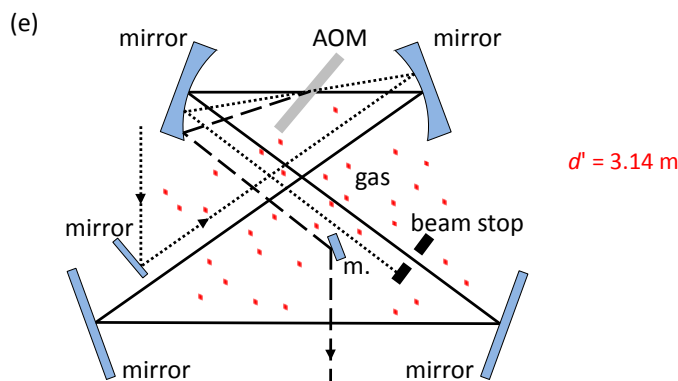
2 Linear (two-mirrors) cavities have also been used for **liquid phase** applications,
 3 where the liquid is either contained in a cuvette or HPLC cell [21,27-29], or enclosed in the
 4 liquid-tight cavity itself (the cavity mirrors acting as windows of the setup) [62]. Islam and
 5 co-workers, for instance, studied liquid analytes with cavities where the high reflectivity con-
 6 cave mirrors were separated by up to 20 cm and sealed with liquid-tight perfluoro polymer O-
 7 rings [62]. With a reported sensitivity of $2.8 \times 10^{-7} \text{ cm}^{-1}$ in a 2.5 s integration time the 20 cm
 8 cavity study demonstrated the potential of IBBCEAS for spectral separation of multiple liq-
 9 uid-phase analytes with overlapping absorption profiles.

10 Neil et al. [76] reported the application of IBBCEAS to *in situ* analyte detection
 11 within microfluidic droplets. In [76] a microfluidic chip was inserted into the optical cavity
 12 normal to the optical axis such that the light within the cavity passes through a single micro-
 13 fluidic channel (Figure 3.1(a.ii)). The number of light passes through the cavity in this ap-
 14 proach is primarily limited by the optical quality of the microfluidic chip itself.

15



16



1
2 **Figure 3.1:** Typical cavity geometries used for broadband cavity-enhanced absorption spec-
3 troscopy. (a) linear cavity: (i) directly filled with gas [5] or liquid [62], (ii) containing a
4 coated or doped substrate [33], or an absorption cell [21] or microfluidic chip [76], (b) prism
5 cavity [77], (c) folded cavity (different internal reflection elements can be used [25,79]), (d)
6 end-coated fiber cavity [65], (e) ring (bow-tie) cavity [68].

8 **Prism cavity**

9 If the width of the spectral coverage in a broadband cavity experiment is important,
10 the high reflectivity range of the mirrors can become the limiting experimental factor. In or-
11 der to overcome this restriction in case a supercontinuum source is available, high finesse opti-
12 cal cavities based on retroreflector prisms with Brewster angle alignment have been intro-
13 duced by Johnston and Lehmann [77] to exploit wavelength independent total internal reflec-
14 tion (Figure 3.1(b)).^{#4} Using a prism cavity the high reflectivity bandwidth is practically only
15 limited by the spectral regions where the prism material exhibits high internal transmission
16 losses. Depending on the prism material (e.g. calcium fluoride - UV/Vis, fused silica -
17 Vis/NIR, barium fluoride NIR) large regions can be covered with high effective reflectivities.
18 Figure 3.1(b) shows the optical cavity designed by Johnston and Lehmann, i.e. two retrore-
19 flectors facing each other such that corresponding faces are parallel. Light enters the cavity at
20 point **1** and exits at **2**. The dimensions, refractive index and angles of the first prism are cho-
21 sen such that a ray entering surface **D** at the Brewster angle will be totally internally reflected
22 at surfaces **A** and **B** at 45°. The second prism is identical except that surface **E** is convex (with
23 a radius of curvature of 6 m in [77]). The input beam passes through surface **C** also at Brew-
24 ster's angle. The effective reflectivity of the cavity is controlled by tuning the input prism
25 around Brewster's angle, yielding [77]:

$$26 \quad R(\lambda) = \frac{(n^4(\lambda) - 1)^2}{4n^6(\lambda)} \delta\theta^2(\lambda), \quad (10)$$

27 where $R(\lambda)$ is the fractional reflected intensity, $n(\lambda)$ is the prism material index of refraction
28 and $\delta\theta(\lambda)$ [rad] is the detuning angle from Brewster's angle. Scattering losses at the prism in-
29 terfaces are minimized by super polishing the optical surfaces ($<1 \text{ \AA}$ rms roughness, scratch-
30 dig 0/0). The calculated Fresnel losses per prism are minimal at the design wavelength of the
31 cavity (1064 nm) and monotonically increased from "negligible" to longer and shorter wave-
32 lengths (to a value of ca. 4 ppm at ~ 650 and ~ 1750 nm in [77]). The round trip time in the

^{#4} High resolution spectra of the weak b-X (1←0) transition of O₂ at 14529 cm⁻¹ and of the fifth overtone of the acetylene C-H stretch vibration at 18430 cm⁻¹ are reported with a FWHM of 0.18 and 0.44 cm⁻¹, respectively.

1 cavity was 3.6 ns for a cavity length of 0.5 m, including the propagation time inside the
2 prisms. More details on the choice of prism material and fabrication errors, optical beam
3 propagation calculations to determine the specification of prism angles and relative dimen-
4 sions, sensitivity of the optic axis to changes in prism alignment and other experimental fea-
5 tures can be found in [78].

7 **Folded cavities for evanescent wave applications**

8 Cavities involving a total internal reflection element (e.g. monolithic or Pellin-Broca
9 cavities and other folded- or ring-cavities) have been applied in numerous evanescent wave
10 (EW) CRDS applications (not including whispering gallery modes in solid microspheres or
11 droplets). A comprehensive review of EW-cavity based spectroscopy (including cavity de-
12 sign and light source considerations as well as applications) has been given recently by
13 Schnippering et al. [79]. For **broadband applications** only **folded cavities** have been used
14 comprising two high reflectivity mirrors and a trapezoidal or right angle prism (Figure
15 3.1(c)). The entrance and exit of the beam are normal to the prism faces, ensuring the reflec-
16 tive losses to be trapped within the cavity [21]. The first broadband (390-625 nm) application
17 demonstrated by Ruth and Lynch [30] used a right angle prism cavity with xenon lamp illu-
18 mination to investigate thin dry films of metallo-porphyrins deposited from solution at the
19 silica-air interface. In this study, a detailed evaluation of the prism losses within the folded
20 cavity is given together with the description of the loss behaviour of an evaporating layer of
21 sample solution. The 3σ minimum loss per pass (ϵd) was found to be 2×10^{-5} for an integra-
22 tion time of 100 ms.

23 An SC source was also applied in conjunction with a folded evanescent-wave cavity for thin
24 layer diagnostic at the interface of a silica substrate [24] to detect electrogenerated species at
25 the silica-water interface in the range 400-750 nm. Schnippering et al. report an effective
26 minimum detectable loss per pass of 3.9×10^{-5} in an integration time of 0.5 s. Real time fast
27 interfacial kinetics of electrogenerated Ir(IV) complexes in a thin-layer electrochemical cell
28 arrangement was shown feasible with a dove prism folded cavity and SC source excitation by
29 van der Sneppen et al. [31].

31 **Other Cavities**

32 An implementation of broadband cavity-enhanced absorption spectroscopy with a 'bow-tie'
33 **ring cavity** (Fig. 3.1(e)) has been demonstrated by Petermann and Fischer for a gas phase
34 application [68]. An intracavity acousto-optic modulator (AOM) is used to directly couple
35 light into (and out-of) the cavity at specified times, however, at the expense of additional
36 losses caused by the AOM. The AOM by-passes the cavity mirrors and makes it possible to
37 load the cavity efficiently and to actively 'dump' the total energy in the cavity at any point
38 onto a photo-detector, enabling a time-dependent CRD approach. The 'bow-tie' geometry
39 helps minimizing the beam waist in the AOM, necessary for fast switching.

40 Other cavity types for broadband absorption enhancement are used for systems on the micro-
41 to nano-scale. Gomez et al. [65] used an **end-coated fibre** for IBCEAS measurements of
42 aqueous samples in nanoliter volumes; the liquid sample is contained within a vertical 100
43 μm wide capillary that is integrated at the center of the horizontal optical fiber (Fig 3.1(d)).
44 Recently the use of low quality factor whispering gallery modes in spherical silicon

1 **nanoshells** has been demonstrated by Yao et al. [80] (Vollmer & Wu in this book). The low
2 quality factor enables good coupling conditions, broadens the resonant absorption peak, and
3 makes the absorption enhancement region wider.

4 **3.2.2 Linear cavity: open-path versus closed-path for *in situ* trace gas monitoring**

5 The largest signal-to-noise enhancements in absorption spectroscopy with cavities can
6 be achieved for gas phase systems. The good time resolution of broadband cavity approaches,
7 in conjunction with a wide spectral coverage at sufficient spectral resolution and their general
8 robustness, are attractive features for *in situ* monitoring of many typical atmospheric trace
9 constituents, either in the natural environment or in atmospheric simulation chambers. Under
10 atmospheric conditions Mie scattering and absorption of aerosol particles can reduce the in-
11 tensity of light in a cavity, apart from molecular absorption of the target species and the elas-
12 tic scattering by air. Aerosol extinction can be accounted for through the analysis of the light
13 attenuation (caused by aerosol) with differential fitting techniques applied to the acquired
14 broadband spectra [50]. The retrieval of species concentration from the spectra is described in
15 detail elsewhere and the reader is referred to refs. [5,33,40,55].

16 Broadband cavity-based instruments with standard linear mirror cavities have been used for
17 atmospherically relevant research either in **open-path** configurations outdoors [12-14], in-
18 doors [50,56,61], or in **simulation chambers** [33,38,44,57,81]), and in **closed-path** configura-
19 tion [43,49,52,54,82,83] by continuously extracting gas from a sample volume and flowing it
20 through an enclosed cavity for detection. Both, open-path and closed-path setups present ad-
21 vantages and drawbacks for trace gas monitoring which will be outlined in the following.

22

23 **Closed-path**

24 Extractive sampling enables the design of compact broadband cavity systems (typi-
25 cally ca. 1 m cavity length) providing good mechanical stability and compactness. Instru-
26 ments can be made portable and can be sheltered inside a small room or container (during
27 measurement campaigns), where thermal stability of the setup components, notably the spec-
28 trometer and optics, can be more easily ensured. A major advantage of enclosed cavities is
29 that any type of calibration procedure, most importantly the *in situ* determination of the mir-
30 ror reflectivity, can be performed in a straightforward manner, by simply filling the cavity
31 with e.g. zero air (for CRD applications) or a calibration gas (for CEAS applications) - see
32 section 3.2.3. Moreover, aerosol optical losses can be eliminated (if required) by filtering the
33 extracted air sample. The main drawback of extractive systems is related to the walls of the
34 setup which are associated with different losses for different target species. Wall losses occur
35 in the inlet line and on the walls of the enclosed cavity over time. The length of the extraction
36 line and the positioning of the instrument with respect to the sampling point is an important
37 consideration; in general short inlet lines are to be preferred. Wall losses of target species in
38 the inlet line, including effects of potential filters or scrubbers and cavity wall losses, which
39 depend on the sample residence time and hence the flow speed settings, need to be thor-
40 oughly considered and require extensive calibration or correction procedures [83,84]. Unfor-
41 tunately for real outdoor gas samples the wall losses may change depending on the composi-
42 tion of the gas mixture and its chemistry, so that some uncertainty of **wall losses** always re-
43 mains. Mirrors are (not necessarily but) typically protected by a small purge flow of zero air
44 or N₂.

Open-path

Instruments operating an open-path cavity have the advantage that they are free from wall losses of target species. Since the cavity mirrors are not enclosed, the length of the cavity can be extended arbitrarily. Provided a bright light source is used that can be well collimated/imaged (cf. section 3.1), the mechanical stability is guaranteed and the gaseous sample is homogeneously distributed between the mirrors, extending the cavity will increase the sensitivity. For instance, in refs. [33,85] an IBBCEAS setup installed at the SAPHIR atmospheric simulation chamber (Jülich, Germany) is described employing a ~20 m long open-path cavity for *in situ* detection of the NO₃ radical between 630 and 690 nm. Using a longer cavity offers the possibility of using mirrors with a lower reflectivity without affecting the sensitivity. Lower mirror reflectivities increase the overall cavity transmission (provided the same amount of light can be coupled through the cavity, e.g. with a SC source) and at the same time enable wider spectral ranges to be covered, which generally improves the retrieval accuracy of target species. Both aerosol extinction and absorption of gaseous molecular and radical species can be retrieved in open-path setups [33,86]. However, in case of a highly variable atmosphere, especially with regard to aerosol load, the concentration retrieval of target species can be challenging. If strong aerosol (or target species) fluctuations occur on a time scale smaller than the experimental integration time, the accuracy of the data analysis is seriously affected. Moreover, for very high aerosol concentrations the molecular absorption signal can be swamped, lowering the effective sensitivity of the open-path design owing to a significant reduction of the effective path length. There is a genuine drawback of open-path configurations which is inherent to all (time- and intensity-dependent) cavity methods using open-path, i.e. a 'clean air' (target species free) reference point (e.g. transmission I_0 in eq. (9) or τ_0 in eq. (3)) is not necessarily available. All concentration measurements including the mirror reflectivity calibration (see section 3.2.3) refer to a reference measurement, which cannot be accurately defined in real outdoor/field environments. In simulation chambers [33,38,44] and other controlled environments where open-path configurations are applied, this issue can be adequately addressed by filling the chamber with zero-air or a calibration gas. For short enough cavities and depending on the experimental design, open-path cavities can be easily turned into closed-path configurations and vice versa, by including and removing a tube between the mirrors. This straightforward feature of having a removable tube incorporated in the cavity, gives the instrument maximum flexibility in terms of reference measurements and calibration. Open-path cavity mirrors are generally also purged with zero-air or N₂. On the detector side of the cavity means for stray light reduction (such as short tubes) are usually implemented for daytime measurements.

3.2.3 Determination of mirror reflectivity

For the measurement of absolute extinction coefficients the (effective) mirror reflectivity, R , needs to be calibrated in case of intensity-dependent methods. This is different from time-dependent approaches where R can be determined through measurements without a sample in the cavity. The calibration is especially critical in broadband techniques where the high reflectivity of low loss mirrors can exhibit significant variations depending on the

1 broadness of the wavelength range. A number of approaches have been established to deter-
 2 mine $R(\lambda)$:

3 (a) Measuring the transmission of a cavity without and with a sample of known con-
 4 centration and **optical loss** (absorption cross-section) leaves only $R(\lambda)$ in eq. (9) an unknown
 5 parameter. The error in the reflectivity depends on the uncertainty of the (resolution cor-
 6 rected) absorption cross-section of the calibration sample apart from the experimental uncer-
 7 tainties associated with determining concentrations and transmission intensities. For atmos-
 8 pheric gas phase measurements typical calibration gases have been NO_2 [38,59] or the dimer
 9 $\text{O}_2\text{-O}_2$ [50,53], and for surface applications organic dyes have been applied [31].

10 (b) Rather than using a molecular absorption loss for calibration the elastic (Rayleigh)
 11 scattering losses of a **calibration** gas (ideally at different pressures) can be used to determine
 12 the mirror reflectivity. For example, Washenfelder et al. determined the reflectivity, $R(\lambda)$, by
 13 measuring the ratio of transmitted intensities when the cavity was filled with He and zero air,
 14 ($I_{\text{air}}/I_{\text{He}}$) [40]. Since Rayleigh scattering cross sections for He and air are well known, the re-
 15 flectivity of the mirrors can be directly determined as

$$16 \quad R(\lambda) = 1 - \left(\frac{\left(\frac{I_{\text{air}}}{I_{\text{He}}} \right) \alpha_r^{\text{air}} - \alpha_r^{\text{He}}}{1 - \left(\frac{I_{\text{air}}}{I_{\text{He}}} \right)} \right) d, \quad (11)$$

17 where α_r^{air} and α_r^{He} denote the extinction coefficients for **Rayleigh scattering** of air and He
 18 respectively.^{#5} The same principle was used by Chen and Venables [43] who used N_2 and
 19 CO_2 . The advantage of this approach is that elastic scattering losses vary uniformly with
 20 wavelength over the entire spectrum, enabling reflectivity measurements over a wide spectral
 21 range covering the near UV and visible.

22 (c) Mirror reflectivities can also be determined by using an antireflection-coated opti-
 23 cal substrate of known loss, $L(\lambda)$, instead of a calibration gas [30,33], which is mostly used in
 24 open-path configurations for calibration and referencing purposes. The reflectivity is then ob-
 25 tained as

$$26 \quad R(\lambda) = 1 - \left(\frac{I_1(\lambda)}{I_0(\lambda) - I_1(\lambda)} L(\lambda) \right), \quad (12)$$

27 where $I_1(\lambda)$ and $I_0(\lambda)$ are the respective transmission spectra of the cavity with and without
 28 the low loss substrate in a clean cavity. $L(\lambda)$ must be determined independently either through
 29 a CRD experiment or through a calibration approach such as (a) or (b).

30 (d) Mirror reflectivity can also be measured if the experimental setup provides the
 31 possibility of a cavity ring-down measurement [15,16]. A few studies have used a type of
 32 "hybrid setup" [29,48,77,87] where CEAS and CRD are combined. Ideally the mirrors do not
 33 need to be changed between the CRD measurement and the broadband CEAS measurement.
 34

35 (e) An alternative "hybrid" calibration approach without altering the cavity alignment
 36 is using PSCRDS, where the mirror reflectivity $R(\lambda)$ is determined directly from phase delay

^{#5} Note that the gases used (He and air) have large differences in their Rayleigh scattering cross sections.

1 measurement $\phi(\lambda)$ [19] introduced in the cavity when purging it with a dry gas
 2 [29,54,82,83,88]:

$$3 \quad R(\lambda) = 1 + d \left(\frac{\Omega}{c \tan \phi(\lambda)} + \alpha(\lambda) \right), \quad (13)$$

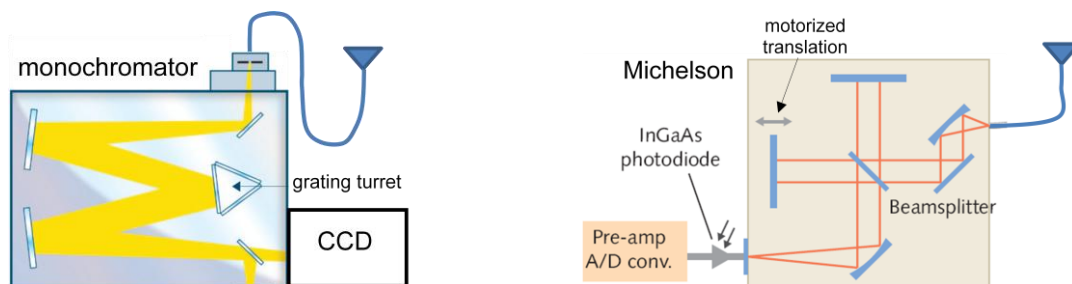
4 where Ω is the angular modulation frequency of the excitation source and α the wavelength-
 5 dependent extinction coefficient due to elastic Rayleigh losses. Mirror reflectivity calibration
 6 using PSCRDS was demonstrated using acousto-optic tunable filters for modulating a single
 7 supercontinuum source, used for both the calibration and the main absorption experiment
 8 [88]. The filters permit narrowband portions of the broadband radiation to be scanned over
 9 the full bandwidth of the cavity mirrors. After the calibration the system is switched over into
 10 a IBBCEAS configuration without any loss in optical alignment.
 11

12 Note that if the full surface area of the mirror is illuminated in a cavity experiment
 13 (typical for IBBCEAS), then the corresponding reflectivity is generally somewhat smaller
 14 than in applications using only on-axis excitation of the cavity. Depending on the cavity ge-
 15 ometry the distribution of modes excited in the cavity determines the reflectivity obtained in
 16 the calibration. Since the contribution of transverse modes is larger if the full mirror is illu-
 17 minated, one essentially measures a (spatial) mean of reflectivities across the mirror surface
 18 for given excitation conditions [51]. This should be kept in mind when different **beam diame-**
 19 **ters** are used for the calibration and the main absorption measurement. The problem of find-
 20 ing a quantitative relationship between the spatial and spectral excitation conditions for a
 21 given cavity geometry and the resulting effective reflectivities of the cavity mirrors has not
 22 been adequately addressed in the literature at the time of publication.
 23

24 **3.3 Detection schemes**

25 All broadband CEA approaches have in common that the wavelength selection takes place
 26 after the cavity^{#6} by either dispersive or interferometric means, as sketched in Figure 3.2.
 27 While the spectral resolution of the setup is solely determined by the type of wavelength se-
 28 lection, the sensitivity is affected by both the wavelength selection scheme and the subse-
 29 quent photo detection efficiency.
 30

31



32

33

34 **Figure 3.2.** Sketches of typical detection schemes. Left: Dispersive approach – grating monochromator and
 35 multi-channel detector (CCD). Right: Interferometric approach – FT spectrometer (Michelson) with single-
 36 channel detector (photodiode or PMT).

^{#6} An exception is the setup in ref. [7] where interferometric processing of the signal was done before the cavity and the transmitted signal was measured immediately after the cavity by a photomultiplier tube.

3.3.1 Dispersive wavelength selection approaches (predominantly near UV to near IR)

The light transmitted through the cavity is either directly focused onto the entrance slit of a monochromator or coupled into a multimode fibre (or fibre bundle) connected to the entrance aperture of a monochromator. The light in the entrance slit is typically imaged onto a (potentially cooled) charged coupled device (CCD) array via a dispersive optical element; typically a reflection grating selecting a single order, see Fig. 3.2. If the diffraction pattern exhibits overlapping orders, then sometimes additional optical filtering is applied to limit the width of the diffraction orders and to avoid the spectral/spatial overlap. Depending on the dispersion of the monochromator the entire broadband spectrum can be acquired simultaneously with a time resolution that is determined by the intensity [W cm^{-2}] on the detector. In case of CCD detector arrays the signal-to-noise ratio is greatly improved by vertical binning of the CCD pixel columns. The monochromator's slit width, the groove density of the grating and its distance from the multi-channel CCD detector determine the spectral resolution in combination with the corresponding pixel size. For IBBCEAS compact monochromators with a few cm focal lengths and modest stray light suppression (typically $10^{-3} \dots 10^{-4}$) are commonly used, providing typical spectral resolutions between ~ 0.1 and ~ 1 nm. This resolution range is sufficient to resolve homogeneously or inhomogeneously broadened spectral features in the UV–VIS as they occur in many molecular environments and systems, e.g. through collisional and Doppler broadened spectra in the gas phase, or through various inhomogeneous broadening mechanisms for molecules on surfaces or in the condensed phase. In these cases spectral interpretation, species monitoring, and diagnostic applications all benefit more from fast detection over a broad wavelength range rather than from a high spectral resolution.

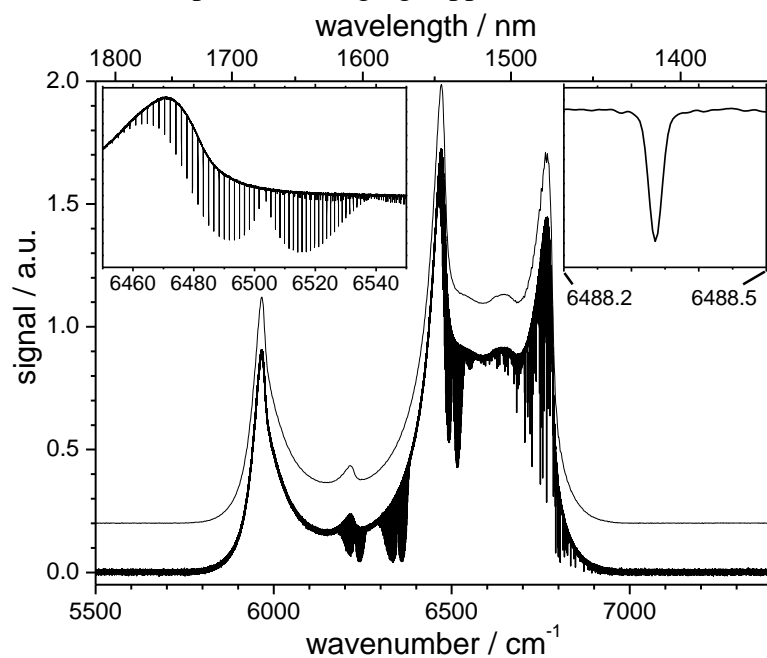
Dispersive wavelength selection methods have been successfully implemented in a wide variety of IBBCEAS applications, including gas phase [8,23,37,61,82,89], liquid phase [21,27–29,62], thin film and surface [24,30,31] studies.

3.3.2 Interferometric wavelength selection approaches (typically in the VIS to near IR)

The light transmitted through the cavity is imaged onto the entrance aperture of a conventional interferometer, which generates an amplitude modulated signal (interferogram) by constructive and destructive interferences of the broadband light travelling over different path lengths inside the interferometer. While a continuously moving (or stepwise scanned) mirror generates optical path differences (δ) between two light beams emerging from the interferometer's beamsplitter, the intensity (I') of the recombined beams is measured by a single detector, typically a (potentially cooled) photodiode or PMT in the focal plane of a positive lens (for interferences localized at infinity). The spectrum $I(\lambda)$ is reconstructed after Fourier transforming the recorded interferogram $I'(\delta)$. The spectral resolution is determined by the combination of both the size of the circular aperture and the maximum optical path difference δ_{max} (i.e. retardation) induced between the two interfering beams. The longer the maximum distance between the moving mirror and the beamsplitter, the higher is the achievable resolution. Typical resolutions reported in the context of broadband cavity experiments are between 0.02 cm^{-1} and 4 cm^{-1} [35,67]. With the option of a much higher spectral resolution than dispersive methods, FTS in conjunction with broadband CEAS has been mainly applied in the (near) IR region, where narrow band ro-vibrational absorption features of molecular species can be exploited to achieve good selectivity. However, high resolution and sensitivity come at the ex-

1 pense of numerous δ scans, which generally require rather long acquisition times. Moreover,
 2 high resolution Fourier transform spectrometers are neither particularly compact, nor very
 3 robust (for field applications) and can furthermore be costly. These aspects illustrate that FT-
 4 IBBCEAS is less appropriate for kinetic studies and for environmental trace gas monitoring
 5 and that its main benefits are in spectroscopic investigations of steady state gas phase sys-
 6 tems. It is especially useful for applications where small sample volumes are required (e.g. in
 7 discharges, combustion plasmas, flames or chemical flow reactors) or where small quantities
 8 of rare and/or expensive compounds (e.g. isotopologues) are of interest.

9 **FT-IBBCEAS** was first demonstrated by Ruth et al. [26] who used a current-stabilized
 10 short-arc Xe lamp as light source. The spin- and symmetry-forbidden B-band of gaseous
 11 oxygen at 688 nm as well as weak absorption transitions of water vapour in ambient air in the
 12 same region were measured in this proof-of-principle study. Further FT-based IBBCEAS
 13 studies include the detection of overtone bands of CO₂, OCS [35], CH₃CN [70] and HD¹⁸O in
 14 the near IR [90]. Using FT-IBBCEAS, sensitivities of $1.5 \times 10^{-8} \text{ cm}^{-1}$ [66] using a fiber cou-
 15 pled SLED and $\sim 4 \times 10^{-9} \text{ cm}^{-1}$ [67] using a **supercontinuum source** have been reported for an
 16 acquisition time of 240 s. It should be noted that fluctuations of the light source as a function
 17 of wavelength are more critical when using an interferometric (FT) detection scheme, be-
 18 cause the noise of the light source is fully transferred to the detector as opposed to a disper-
 19 sive approach where an inherent "spectral averaging" applies.



20
 21
 22 **Figure 3.3.** High-resolution spectrum of CO₂ in the near IR obtained using an optical cavity in conjunction with
 23 a Fourier-transform spectrometer (a.u. = arbitrary units of intensity) [35]. The upper trace (shifted upwards for
 24 clarity) shows the spectrum of the empty cavity, the lower trace shows the spectrum obtained with 26.7 mbar of
 25 CO₂ in the cavity. The acquisition time is 90 min, the spectral resolution is 0.02 cm^{-1} . The inset in the left upper
 26 corner shows a weak overtone band ($30^0_1 \leftarrow 00^0_0$) of CO₂ centered at 6503.08 cm^{-1} , and the inset in the right
 27 upper corner shows the P(18) line in this band to illustrate the signal-to-noise ratio, the spectral resolution, and
 28 the symmetry of the instrumental line shape.

29
 30 Figure 3.3 shows moderately strong bands of the $14^0_1 \leftarrow 00^0_0$, $22^0_1 \leftarrow 00^0_0$ and $30^0_1 \leftarrow 00^0_0$
 31 transitions of the Fermi tetrad of CO₂ centred at $\sim 6227 \text{ cm}^{-1}$, 6347 cm^{-1} and 6503 cm^{-1} , re-
 32 spectively [91], measured using FT-IBBCEAS [35]. There are also some associated hot bands
 33 as well as water absorption lines in the $1.6 \mu\text{m}$ region. This example demonstrates another

1 advantage of combining broad-band coverage (ca. 1200 cm^{-1} in Fig. 3.3) with **high spectral**
 2 **resolution** (and high sensitivity). The zero absorption baseline (I_0) and the transmitted inten-
 3 sity with target species (I) can be performed simultaneously as long as the observed line den-
 4 sity is low enough for I_0 to be unambiguously observable. This experimental feature strongly
 5 reduces the systematic error on the resultant absolute molecular absorption cross-sections.
 6 Moreover, an effective mirror reflectivity measurement becomes possible if a calibration gas
 7 (such as CO_2) is present in the cavity or can be added to the experimental gas mixture (the
 8 **calibration** gas spectrum can obviously be used for wavelength calibration at the same time).

9 If the partial pressure of the calibration gas is known (P_{cal} [Pa]), R can be determined
 10 from the known integrated line intensity of the calibration gas (S_{cal} [cm molecule^{-1}]). Let d
 11 [cm] be the cavity length, T [K] the temperature, and k the Boltzmann constant, then the (ef-
 12 fective) **reflectivity** as a function of maximal absorption wavenumbers ($\tilde{\nu}_{\text{max}}$ [cm^{-1}]) of the
 13 calibration gas is given by [35]:

$$14 \quad R(\tilde{\nu}_{\text{max}}) = 1 - \frac{d \times \frac{P_{\text{cal}}}{kT} \times S_{\text{cal}}(\tilde{\nu}_{\text{max}})}{\int_{\tilde{\nu}_0}^{\tilde{\nu}_0 + \Delta\tilde{\nu}} \left(\frac{\bar{I}_0(\Delta\tilde{\nu})}{I_{\text{cal}}(\tilde{\nu})} - 1 \right) d\tilde{\nu}}, \quad (14)$$

15 where $I_{\text{cal}}(\tilde{\nu})$ is the intensity transmitted through the cavity on an absorption line of the cali-
 16 bration gas at wavenumber $\tilde{\nu}$, and $\bar{I}_0(\Delta\tilde{\nu})$ is the zero-absorption baseline averaged over a
 17 small wavenumber interval $\Delta\tilde{\nu}$ in the vicinity of corresponding absorption line of the calibra-
 18 tion gas. $\tilde{\nu}_0$ is a spectral position off the absorption line ($\tilde{\nu}_0 < \tilde{\nu}_{\text{max}}$) that defines the integral
 19 boundaries in eq. (14). The choice of the integration limits depends on the line profile and
 20 **line width**. For example, in the case of a Lorentzian line shape (with broad wings) integration
 21 over 6 half widths at half maximum (HWHM) yields only 91% of the line area. In such cases,
 22 fitting of the measured data with an analytical expression for the line profile might be helpful,
 23 but requires knowledge of the line shape and, if possible, a negligible (or well known) contri-
 24 bution of the instrument function.

25 3.3.3 Detection limit

26 The integration time corrected **noise-equivalent extinction coefficient**, ε_{nec} , at a given wave-
 27 length (typically taken at the maximal mirror reflectivity) is defined as the minimal extinction
 28 coefficient, ε_{min} [cm^{-1}], that can be measured reliably by the instrument, multiplied by the
 29 square root of the integration time, $t_{\text{int}}^{1/2}$ [$\text{Hz}^{-1/2}$]. The resulting noise-equivalent extinction co-
 30 efficient at λ is independent of the integration time and can thus be compared for instruments
 31 using different detection methods:

$$32 \quad \varepsilon_{\text{nec}}(\lambda) = \varepsilon_{\text{min}}(\lambda) \times t_{\text{int}}^{1/2}. \quad (15)$$

33
 34 For IBCEAS the minimum extinction coefficient, ε_{min} , depends on the minimal detectable
 35 intensity difference ($\Delta I_{\text{min}} = (I_0 - I)_{\text{min}}$) and can be written as (cf. section 2.3.1) [21,22]:
 36

$$\varepsilon_{\min}(\lambda) \geq \frac{1}{d} \left(\frac{\Delta I_{\min}(\lambda)}{I(\lambda)} \right) (1 - R(\lambda)). \quad (16)$$

In eq. (16) the '=' sign corresponds to a **signal-to-noise ratio** of 1, which does not serve as a particularly meaningful limit of detection. In practice, the minimal detectable intensity variation $\Delta I_{\min}(\lambda)$ is established considering the 3σ standard deviation of a statistically significant data set of transmissions of a target-free cavity.

Increasing the integration time t_{int} generally increases the signal-to-noise ratio (**SNR**) and therefore minimizes the noise-equivalent extinction coefficient up to a certain limit that depends on the way different forms of noise affect the measurement. The noise in cavity-enhanced absorption experiments is generally **not** dominated by detector noise (i.e. readout noise and dark noise), because the application of a cavity (which inherently lowers light intensities substantially) requires the detector noise to be smaller than the photon noise in order to achieve an enhancement. Many IBBCEAS experiments are **photon noise**-limited (also termed "quantum noise" or "shot noise") for reasonably short integration times, . In this case the SNR is proportional to $t_{\text{int}}^{1/2}$ up to a time where other forms of noise (e.g. light source fluctuations, mechanical stabilities, thermal drifts and others) start dominating the noise. Beyond that point, the detection is said to be "instrumental" or "environmental" noise-limited [92].^{#7} The two regimes are illustrated in Figure 3.4(a) where the species-specific limit of detection (see below) is shown as a function of integration time.

The **species-specific limit of detection (LOD)** depends additionally on the retrieval procedure applied to the measured extinction spectra. The extinction coefficient $\varepsilon(\lambda)$ can be expressed in a general form as:

$$\varepsilon(\lambda) = \sum_i \sigma_i(\lambda) \int_0^{d'} n_i(x) dx + \varepsilon_{\text{backgr}}(\lambda), \quad (17)$$

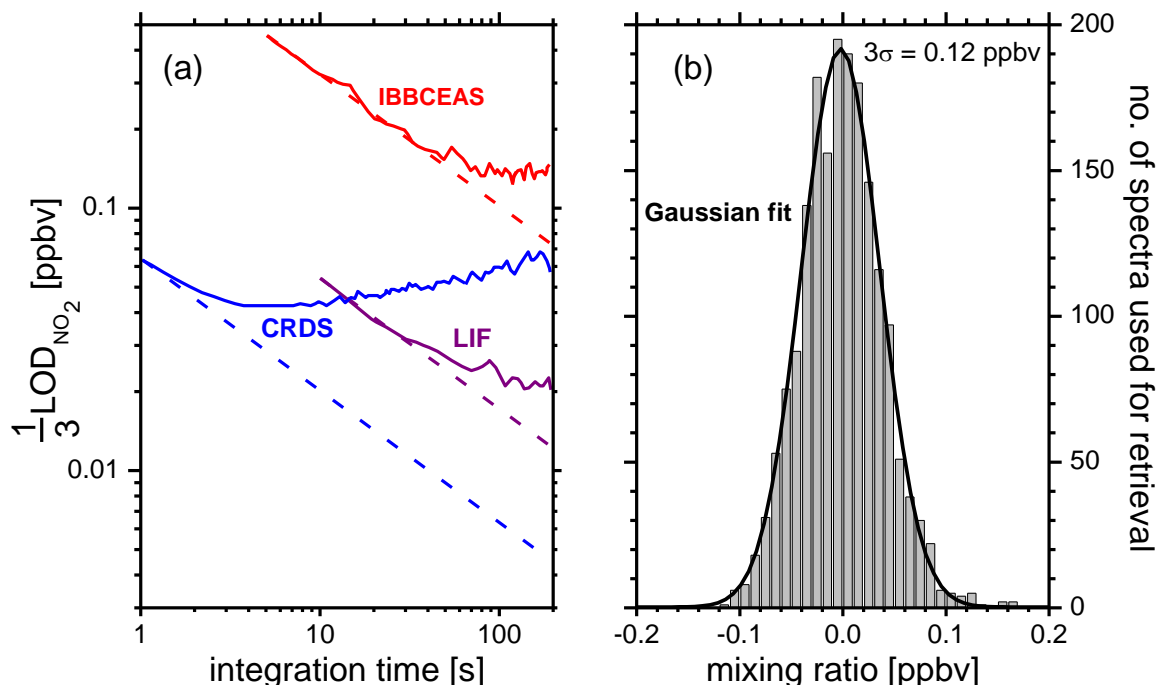
where $\sigma_i(\lambda)$ and n_i are the cross-section and number density of species i at λ , while the second term, $\varepsilon_{\text{backgr}}(\lambda)$, accounts for any unspecified ("extinction") background. Knowledge of $\sigma_i(\lambda)$ from reference databases (e.g. HITRAN, PNNL, GEISA and others) and appropriate modelling of $\varepsilon_{\text{backgr}}(\lambda)$ (e.g. by an adequate polynomial), enables the fitting of eq. (17) to measured extinction data for the retrieval of number densities (commonly also expressed as mixing ratios) of sample species i . The retrieval procedure depends on the method used for least square minimization, on the choice of the final form of eq. (17), on the reliability of the reference cross-sections and their convolution to instrumental resolution, and finally on the wavelength range used for the retrieval. Retrieval methods will not be discussed here – more details can be found in refs. [5,33,55]. The species-specific LOD can be defined as the number density of a given species i that can be reliably retrieved for a certain integration time, t_{int} :

$$\text{LOD}_i(t_{\text{int}}) \geq \Delta n_{i,\min} \quad (18)$$

where $\Delta n_{i,\min}$ is the 3σ deviation of the (typically Gaussian) distribution of number densities retrieved for a target-free cavity. This distribution can be obtained from a statistically signifi-

^{#7} The "instrumental/environmental" noise does not include systematic error sources and needs to be considered from experiment to experiment.

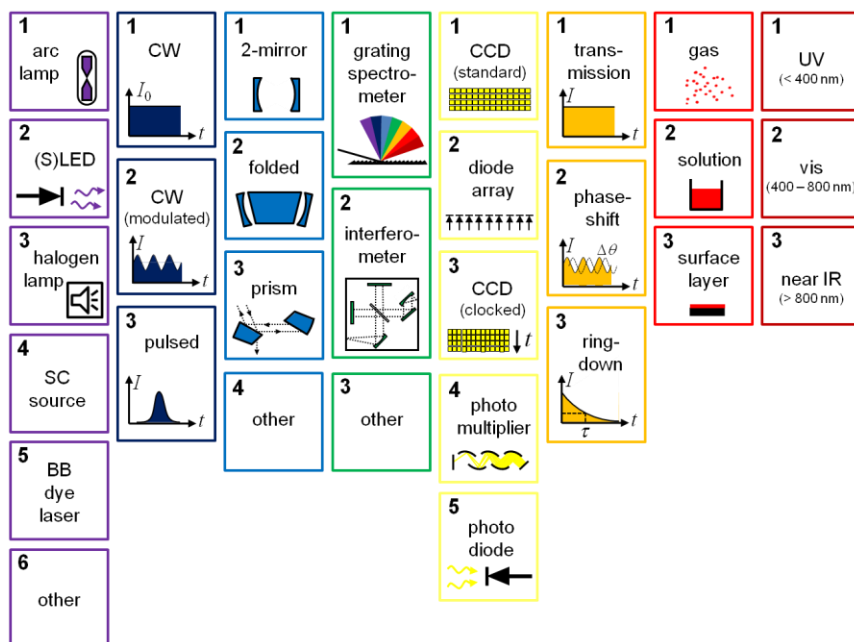
1 cant number of measured spectra in the target-free cavity (for atmospheric applications typi-
 2 cally flushed with zero-air). From each of these spectra, number densities of all target species
 3 accounted for in eq. (17) are retrieved simultaneously. An example is shown Figure 3.4(b) for
 4 an open-path IBBCEAS instrument that has been implemented at the SAPHIR atmospheric
 5 chamber for the near-UV detection of NO₂ and HONO.



6
 7 **Figure 3.4.** (a) Log-log plot of the 1σ signal-to-noise ratio ($=1/3$ LOD) of the target-free (zero-air) SAPHIR
 8 chamber in Jülich versus integration time for three different instruments (IBBCEAS, CRDS and laser induced
 9 fluorescence (LIF)). Data were determined during the NO₃comp campaign in 2007 [33,85] and the figure was
 10 adapted from ref. [84]. The main IBBCEAS target species were NO₃, NO₂ and H₂O. The spectral evaluation
 11 region for NO₂ was 630-645 nm. The optimum integration time for the IBBCEAS setup is ca. 100 s. (b) The
 12 viewgraph shows the number of zero-air spectra taken with an IBBCEAS instrument at SAPHIR in 2011 (1800
 13 in total over 30 discontinued hours) as a function of the retrieved NO₂ mixing ratios. The 3σ value of the Gaus-
 14 sian distribution represents the LOD for NO₂ of 0.12 ppbv for a 1 min integration time. The LOD depends on
 15 the spectral range covered (352-386 nm) and on the retrieval method (which in the present case also included
 16 the target species HONO).

17 4. Summary of literature

18 The table below summarizes the main literature on **broadband cavity-enhanced absorption**
 19 **methods with incoherent light sources**. The literature is ordered according to an 8-digit
 20 code which can be looked up in the diagram above the table. The code represents the combi-
 21 nation of the following experimental parameters: light source, (time-)mode, cavity type,
 22 wavelength selection method, detector type, measurement principle, phase of the target sam-
 23 ple, and spectral range. The listed literature does **not** comprise spectroscopic approaches in-
 24 volving frequency combs, for instance in mode-locked cavity-enhanced absorption spectro-
 25 scopy [1,93-95], in cavity-enhanced femtosecond frequency comb spectroscopy [96-99] or in
 26 vernier spectroscopy [100,101]. It neither covers cavity approaches involving whispering gal-
 27 lery mode resonators which will be dealt with in chapters (Maslowski & Ye) and (Vollmer
 28 & Wu) of this book, respectively.



2

Light source	Mode	Cavity	Wave-length selection	Detector	Exp. method	Sample phase	Spectral range	References
1	1	1	1	1	1	1	1	[43,44]
1	1	1	1	1	1	1	2	[33,38-42,81,84-86]
1	1	1	1	1	1	2	2	[21, 102]
1	1	1	1	2	1	1	2	[8,37]
1	1	1	2	5	1	1	2	[26]
1	1	1	2	5	1	1	3	[35,90]
1	1	2	1	2	1	3	2	[30]
1	2	1	2	4	2	1	2	[7]
1 ^a	3	1	1	1	1	1	2	[45]
1	3	1	1	1	1	1	2	[75]
2	1	1	1	1	1	1	1	[59-61,89,103]
2	1	1	1	1	1	1	2	[48 ^h ,49-54,56,57,82 ^h ,83 ^h ,85,89]
2	1	1	1	1	1	2	2	[27,28,62]
2	1	1	2	5	1	1	3	[66,67]
2	1	2	1	1	1	3	2	[31]
2	1	4 ^b	3	5	1	2	3	[65]
2	2 ^c	1	1	5 ^c	1	1	3	[66]
2	2	1	3	4	2	1	2	[63]
2	2	1	3	5	2	1	2	[64,104]
2	3	1	1	1	1	1	1	[58]
2	3 ^d	4	1	1	3	1	2	[68]
3	1	1	1	4	1	2	2	[21]
3	1	1	3	4	1	1	2	[46]
4	3	1	1	1	1	1	2	[23,88 ^h]
4	3	1	1	1	1	2	2	[29 ^h ,76]
4	3	1	1	1	3	1	2	[15,17]
4	3	1	1	2	3	2	2	[18]
4	3	1	1	4	3	1	2	[16]
4	3	1	1 ^e	? ^e	1	1	3	[87 ^h]
4	3	1	2	5	1	1	3	[67,70]
4	3	1	3	4	3	2	2	[18]
4	3	2	1	1	1	3	2	[24,31]
4	3	3	1	1	1	1	2	[77 ^h]
5	3	1	1	1	1	1	2	[105]
5	3	1	1	1	3	1	2	[10,72,106]
5	3	1	1	3	3	1	2	[6,12-14,84,85,107]
5	3	1	2	4	3	1	2	[73]
6 ^f	3	1	1	5	3	1	3	[74]

3 ^aPlasma self-absorption in a pulsed jet4 ^bEnd-coated fiber cavity5 ^cMechanical chopper modulation and lock-in (phase sensitive) detection6 ^dAn intracavity acousto-optic modulator (AOM) was used to directly couple light into (and out-of) the cavity7 ^eWavelength selection and light detection were integrated into a commercialized optical spectrum analyser (ASO, Yokogawa AQ6317Q)8 ^hHigh repetition rate free electron laser9 ^hHybrids where different experimental approaches are used for calibration and main absorption measurements

References

- [1] Gherman, T., Romanini, D.: Mode-locked cavity-enhanced absorption spectroscopy. *Opt. Expr.* **10**, 1033-1042 (2002)
- [2] O'Keefe, A.: Integrated cavity output analysis of ultra-weak absorption. *Chem. Phys. Lett.* **293**, 331-336 (1998)
- [3] Lehmann, K.K., Romanini, D.: The superposition principle and cavity ring-down spectroscopy. *J. Chem. Phys.* **105**, 10263-10277 (1996)
- [4] Ball, S.M., Jones, R.L.: Broad-band cavity ring-down Spectroscopy. *Chem. Rev.* **103**, 5239-5262 (2003)
- [5] Ball, S., Jones, R.: Broadband cavity ring-down spectroscopy, in *Cavity Ring Down Spectroscopy: Techniques and Applications*. Editors G. Berden and R. Engeln. Wiley, ISBN: 978-1-4051-7688-0 (2009)
- [6] Ball, S.M., Povey, I.M., Norton, E.G., Jones, R.L.: Broadband cavity ring-down spectroscopy of the NO₃ radical. *Chem. Phys. Lett.* **342**, 113-120 (2001)
- [7] Hamers, E., Schram, D., Engeln, R.: Fourier transform phase shift cavity ring down spectroscopy. *Chem. Phys. Lett.* **365**, 237-243 (2002)
- [8] Fiedler, S.E., Hese, A., Ruth, A.A.: Incoherent broad-band cavity-enhanced absorption spectroscopy. *Chem. Phys. Lett.* **371**, 284-294 (2003)
- [9] O'Keefe, A., Deacon, D.A.G.: Cavity ring-down optical spectrometer for absorption measurements using pulsed laser sources. *Rev. Sci. Instrum.* **59**, 2544-2554 (1988)
- [10] Scherer, J.J., Paul, J.B., Jiao, H., O'Keefe, A.: Broadband ringdown spectral photography, *Appl. Opt.* **40**, 6725-6732 (2001)
- [11] Povey, I.M., South, A.M., t'Kint de Roodenbeke, A., Hill, C., Freshwater, R.A., Jones, R.L.: A broadband lidar for the measurement of tropospheric constituent profiles from the ground. *J. Geophys. Res.* **103**, 3369-3380 (1998)
- [12] Bitter, M., Ball, S.M., Povey, I.M., Jones, R.L.: A broadband cavity ringdown spectrometer for in-situ measurements of atmospheric trace gases. *Atm. Chem. Phys.* **5**, 2547-2560 (2005)
- [13] Saiz-Lopez, A., et al.: Modelling molecular iodine emissions in a coastal marine environment: the link to new particle formation. *Atmos. Chem. Phys.* **6**, 883-895 (2006)
- [14] Leigh, R.J., et al.: Measurements and modelling of molecular iodine emissions, transport and photodestruction in the coastal region around Roscoff. *Atmos. Chem. Phys.* **10**, 11823-11838 (2010)
- [15] Schmidl, G., Paa, W., Triebel, W., Schippel, S., Heyer, H.: Spectrally resolved cavity ring down measurement of high reflectivity mirrors using a supercontinuum laser source. *Appl. Opt.* **48**, 6754-6759 (2009)
- [16] Stelmaszczyk, K., Fechner, M., Rohwetter, P., Queißer, M., Czyżewski, A., Stacewicz, T., Wöste, L.: Towards Supercontinuum Cavity Ring-Down Spectroscopy. *Appl. Phys. B* **94**, 369-373 (2009)
- [17] Stelmaszczyk, K., Rohwetter, P., Fechner, M., Queißer, M., Czyżewski, A., Stacewicz, T., Wöste, L.: Cavity ring-down absorption spectrography based on filament-generated supercontinuum light. *Opt. Expr.* **17**, 3673-3678 (2009)

- 1 [18] Kiwanuka, S.S., Laurila T.K., Frank J.H., Esposito, A., Blomberg von der Geest, K.,
2 Pancheri, L., Stoppa, D., Kaminski, C.F.: Development of broadband cavity ring-
3 down spectroscopy for biomedical diagnostics of liquid analytes. *Anal. Chem.* **84**,
4 5489-5493 (2012)
- 5 [19] Herbelin, J.M., McKay, J.A., Kwok, M.A., Ueunten, R.H., Urevig, D.S., Spencer,
6 D.J., Benard, D.J.: Sensitive measurement of photon lifetime and true reflectances in
7 an optical cavity by a phase-shift method. *Appl. Opt.* **19**, 144-147 (1980)
- 8 [20] Engeln, R., von Helden, G., Berden, G., Meijer, G.: Phase shift cavity ring down ab-
9 sorption spectroscopy. *Chem. Phys. Lett.* **262**, 105-109 (1996)
- 10 [21] Fiedler, S.E., Hese, A., Ruth, A.A.: Incoherent broad-band cavity-enhanced absorp-
11 tion spectroscopy of liquids. *Rev. Sci. Instrum.* **76**, 023107 (2005) and erratum **76**
12 (2005) 089901.
- 13 [22] Fiedler, S.E., Hese, A., Heitmann, U.: Influence of the cavity parameters on the output
14 intensity in incoherent broadband cavity-enhanced absorption spectroscopy. *Rev. Sci.*
15 *Instrum.* **78**, 073104 (2007)
- 16 [23] Langridge, J.M., Laurila, T., Watt, R.S., Jones, R.L., Kaminski, C.F., Hult, J.: Cavity
17 enhanced absorption spectroscopy of multiple trace gas species using a
18 supercontinuum radiation source. *Opt. Expr.* **16**, 10178-10188 (2008)
- 19 [24] Schnippering, M., Unwin, P.R., Hult, J., Laurila, T., Kaminski, C.F., Langridge, J.M.,
20 Jones, R.L., Mazurenka, M., Mackenzie, S.R.: Evanescent wave broadband cavity en-
21 hanced absorption spectroscopy using supercontinuum radiation: A new probe of
22 electrochemical processes. *Electrochem. Commun.* **10**, 1827-1830 (2008)
- 23 [25] Lynch, K.: Incoherent broad-band cavity-enhanced total internal reflection spectros-
24 copy of surface-adsorbed metallo-porphyrins. PhD thesis, Physics Department, Uni-
25 versity College Cork, Ireland (2008)
- 26 [26] Ruth, A.A., Orphal, J., Fiedler, S.E.: Fourier-transform cavity-enhanced absorption
27 spectroscopy using an incoherent broadband light source. *Appl. Opt.* **46**, 3611-3616
28 (2007)
- 29 [27] Islam, M., Seetohul, L.N., Ali, Z.: Liquid-phase broadband cavity-enhanced absorp-
30 tion spectroscopy measurements in a 2 mm cuvette. *Appl. Spectrosc.* **61**, 649-658
31 (2007)
- 32 [28] Seetohul, L.N., Ali, Z., Islam, M.: Broadband cavity enhanced absorption spectrosc-
33 ophy as a detector for HPLC, *Anal. Chem.* **81**, 4106-4112 (2009)
- 34 [29] Kiwanuka, S.S., Laurila, T., Kaminski, C.F.: Sensitive method for the kinetic meas-
35 urement of trace species in liquids using cavity enhanced absorption spectroscopy
36 with broad bandwidth supercontinuum radiation. *Anal. Chem.* **82**, 7498-7501 (2010)
- 37 [30] Ruth, A.A., Lynch, K.T.: Incoherent broadband cavity-enhanced total internal reflec-
38 tion spectroscopy of surface adsorbed metalloporphyrins. *Phys. Chem. Chem. Phys.*
39 **10**, 7098-7108 (2008)
- 40 [31] Van der Sneppen, L., Hancock, G., Kaminski, C., Laurila, T., Mackenzie, S.R., Neil,
41 S.R.T., Peverall, R., Ritchie, G.A.D., Schnippering, M., Unwin, P.R.: Following inter-
42 facial kinetics in real time using broadband evanescent wave cavity-enhanced absorp-
43 tion spectroscopy: a comparison of light-emitting diodes and supercontinuum sources.
44 *Analyst* **135**, 133-139 (2010)

- 1 [32] Wilbers, A.T.M., Kroesen, G.M.W., Timmermans, C.J., Schram, D.C.: The continu-
2 um emission of an arc plasma. *J. Quant. Spectrosc. Radiat. Transf.* **45**, 1-10 (1991)
- 3 [33] Varma, R.M., Venables, D.S., Ruth, A.A., Heitmann, U., Schlosser, E., Dixneuf, S.:
4 Long optical cavities for open-path monitoring of atmospheric trace gases and aerosol
5 extinction. *Appl. Opt.* **48**, B159-171 (2009)
- 6 [34] Welz, B., Becker-Ross, H., Florek, S., Heitmann, U.: *High-resolution continuum*
7 *source AAS: the better way to do atomic absorption spectrometry* (Wiley VCH, 2005)
- 8 [35] Orphal, J., Ruth, A.A.: High-resolution Fourier-transform cavity-enhanced absorption
9 spectroscopy in the near-infrared using an incoherent broad-band light source. *Opt.*
10 *Expr.* **16**, 19232-19243 (2008)
- 11 [36] Platt, U., Stutz, J.: *Differential Optical Absorption Spectroscopy: Principles and Ap-*
12 *plications*. Springer, Berlin (2008)
- 13 [37] Fiedler, S.E., Hoheisel, G., Ruth, A.A., Hese, A.: Incoherent broad-band cavity-
14 enhanced absorption spectroscopy of azulene in a supersonic jet. *Chem. Phys. Lett.*
15 **382**, 447-453 (2003)
- 16 [38] Venables, D.S., Gherman, T., Orphal, J., Wenger, J.C., Ruth, A.A.: High sensitivity *in*
17 *situ* monitoring of NO₃ in an atmospheric simulation chamber using incoherent
18 broadband cavity-enhanced absorption spectroscopy. *Environ. Sci. Technol.* **40**, 6758-
19 6763 (2006)
- 20 [39] Vaughan, S., Gherman, T., Ruth, A.A., Orphal, J.: Incoherent broad-band cavity-
21 enhanced absorption spectroscopy of the marine boundary layer species I₂, IO and
22 OIO. *Phys. Chem. Chem. Phys.* **10**, 4471-4477 (2008)
- 23 [40] Washenfelder, R.A., Langford, A.O., Fuchs, H., Brown, S.S.: Measurement of glyoxal
24 using an incoherent broadband cavity enhanced absorption spectrometer. *Atmos.*
25 *Chem. Phys.* **8**, 7779-7793 (2008)
- 26 [41] Dixneuf, S., Ruth, A.A., Vaughan, S., Varma, R.M., Orphal J.: The time dependence
27 of molecular iodine emission from *Laminaria digitata*. *Atmos. Chem. Phys.* **9**, 823-
28 829 (2009)
- 29 [42] Nitschke, U., Ruth, A.A., Dixneuf, S., Stengel, D.B.: Molecular iodine emission rates
30 and photosynthetic performance of different thallus parts of *Laminaria digitata*
31 (Phaeophyceae) during emersion. *Planta* **233**, 737-748 (2011)
- 32 [43] Chen, J., Venables, D.S.: A broadband optical cavity spectrometer for measuring
33 weak near-ultraviolet absorption spectra of gases. *Atmos. Meas. Tech.* **4**, 425-436
34 (2011)
- 35 [44] Chen, J., Wenger, J.C., Venables, D.S.: Near-ultraviolet absorption cross sections of
36 nitrophenols and their potential influence on tropospheric oxidation capacity. *J. Phys.*
37 *Chem. A* **115**, 12235-12242 (2011)
- 38 [45] Walsh, A., Zhao, D., Linnartz, H.: Cavity enhanced plasma self-absorption spectros-
39 copy. *Appl. Phys. Lett.* **101**, 091111 (2012)
- 40 [46] Thompson, J.E., Spangler, H.D.: Tungsten source integrated cavity output spectrosc-
41 ophy for the determination of ambient atmospheric extinction coefficient. *Appl. Opt.* **45**,
42 2465-2473 (2006)
- 43 [47] Kern, C., Trick, S., Rippel, B., Platt, U.: Applicability of light-emitting diodes as light
44 sources for active differential optical absorption spectroscopy measurements. *Appl.*
45 *Opt.* **45**, 2077-2088 (2006)

- 1 [48] Ball, S.M., Langridge, J.M., Jones, R.L.: Broadband cavity enhanced absorption spectroscopy using light emitting diodes. *Chem. Phys. Lett.* **398**, 68-74 (2004)
- 2
- 3 [49] Ventrillard-Courtilot, I., Sciamma O'Brien, E., Kassi, S., Méjean, G., Romanini, D.: Incoherent broad-band cavity-enhanced absorption spectroscopy for simultaneous trace measurements of NO₂ and NO₃ with a LED source. *Appl. Phys. B* **101**, 661-669 (2010)
- 4
- 5
- 6
- 7 [50] Langridge, J.M., Ball, S.M., Jones, R.L.: A compact broadband cavity enhanced absorption spectrometer for detection of atmospheric NO₂ using light emitting diodes. *Analyst* **131**, 916-922 (2006)
- 8
- 9
- 10 [51] Triki, M., Cermak, P., Méjean, G., Romanini, D.: Cavity-enhanced absorption spectroscopy with a red LED source for NO_x trace analysis. *Appl. Phys. B* **91**, 195-201 (2008)
- 11
- 12
- 13 [52] Wu, T., Zhao, W., Chen, W., Zhang, W., Gao, X.: Incoherent broadband cavity enhanced absorption spectroscopy for *in situ* measurements of NO₂ with a blue light emitting diode. *Appl. Phys. B* **94**, 85-94 (2009)
- 14
- 15
- 16 [53] Ball, S.M., Hollingsworth, A.M., Humbles, J., Leblanc, C., Potin, P., McFiggans, G.: Spectroscopic studies of molecular iodine emitted into the gas phase by seaweed. *Atmos. Chem. Phys.* **10**, 6237-6254 (2010)
- 17
- 18
- 19 [54] Benton, A.K., Langridge, J.M., Ball, S.M., Bloss, W.J., Dall'Osto, M., Nemitz, E., Harrison, R.M., Jones, R.L.: Night-time chemistry above London: measurements of NO₃ and N₂O₅ from the BT Tower. *Atmos. Chem. Phys.* **10**, 9781-9795 (2010)
- 20
- 21
- 22 [55] Platt, U., Meinen, J., Pöhler, D., Leisner, T.: Broadband cavity enhanced differential optical absorption spectroscopy (CE-DOAS) – applicability and corrections. *Atmos. Meas. Tech.* **2**, 713-723 (2009)
- 23
- 24
- 25 [56] Thalman, R., Volkamer, R.: Inherent calibration of a blue LED-CE-DOAS instrument to measure iodine oxide, glyoxal, methyl glyoxal, nitrogen dioxide, water vapour and aerosol extinction in open cavity mode. *Atmos. Meas. Tech.* **3**, 1797-1814 (2010)
- 26
- 27
- 28 [57] Meinen, J., Thieser, J., Platt, U., Leisner, T.: Technical Note: Using a high finesse optical resonator to provide a long light path for differential optical absorption spectroscopy: CE-DOAS. *Atmos. Chem. Phys.* **10**, 3901-3914 (2010)
- 29
- 30
- 31 [58] Hoch, D. J., Buxmann, J., Sihler, H., Pöhler, D., Zetzsch, C., Platt, U.: A cavity-enhanced differential optical absorption spectroscopy instrument for measurement of BrO, HCHO, HONO and O₃. *Atmos. Meas. Tech. Discuss.* **5**, 3079-3115 (2012)
- 32
- 33
- 34 [59] Gherman, T., Venables, D.S., Vaughan, S., Orphal, J., Ruth, A.A: Incoherent broadband cavity-enhanced absorption spectroscopy in the near-ultraviolet: Application to HONO and NO₂. *Environ. Sci. Technol.* **42**, 890-895 (2008)
- 35
- 36
- 37 [60] Roberts, J.M., Veres, P., Warneke, C., Neuman, J.A., Washenfelder, R.A., Brown, S.S., Baasandorj, M., Burkholder, J.B., Burling, I.R., Johnson, T.J., Yokelson, R.J., de Gouw, J.: Measurement of HONO, HNCO, and other inorganic acids by negative-ion proton-transfer chemical-ionization mass spectrometry (NI-PT-CIMS): application to biomass burning emissions. *Atmos. Meas. Tech. Discuss.* **3**, 301-331 (2010)
- 38
- 39
- 40
- 41
- 42 [61] Wu, T., Chen, W., Fertein, E., Cazier, F., Dewaele, D., Gao, X.: Development of an open-path incoherent broadband cavity-enhanced spectroscopy based instrument for simultaneous measurement of HONO and NO₂ in ambient air. *Appl. Phys. B* **106**, 501-509 (2012)
- 43
- 44
- 45

- 1 [62] Seetohul, L.N., Ali, Z., Islam, M.: Liquid-phase broadband cavity enhanced absorption spectroscopy (BBCEAS) studies in a 20 cm cell. *Analyst* **134**, 1887-1895 (2009)
- 2
- 3 [63] Kebabian, P.L., Herndon, S.C., Freedman, A.: Detection of nitrogen dioxide by cavity attenuated phase shift spectroscopy. *Anal. Chem.* **77**, 724-728 (2005)
- 4
- 5 [64] Kebabian, P.L., Wood, E.C., Herndon, S. C., Freedman, A.: A practical alternative to chemiluminescence-based detection of nitrogen dioxide: cavity attenuated phase shift spectroscopy. *Environ. Sci. Technol.* **42**, 6040-6045 (2008)
- 6
- 7
- 8 [65] Gomez, A.L., Renzi, R.F., Fruetel, J.A., Bambha, R.P.: Integrated fiber optic incoherent broadband cavity enhanced absorption spectroscopy detector for near-IR absorption measurements of nanoliter samples. *Appl. Opt.* **51**, 2532-2540 (2012)
- 9
- 10
- 11 [66] Denzer, W., Hamilton, M.L., Hancock, G., Islam, M., Langley, C. E., Peverall, R., Ritchie, G.A.D.: Near-infrared broad-band cavity enhanced absorption spectroscopy using a superluminescent light emitting diode. *Analyst* **134**, 2220-2023 (2009)
- 12
- 13
- 14 [67] Denzer, W., Hancock, G., Islam, M., Langley, C.E., Peverall, R., Ritchie G.A.D., Taylor, D.: Trace species detection in the near infrared using Fourier transform broadband cavity enhanced absorption spectroscopy: initial studies on potential breath analytes. *Analyst* **136**, 801-806 (2011) and erratum **136**, 5308 (2011).
- 15
- 16
- 17
- 18 [68] Petermann, C., Fischer P.: Actively coupled cavity ringdown spectroscopy with low-power broadband sources. *Opt. Expr.* **19**, 10164-10173 (2011)
- 19
- 20 [69] Dudley, J.M., Genty, G., Coen, S.: Supercontinuum generation in photonic crystal fiber. *Rev. Mod. Phys.* **78**, 1135-1184 (2006)
- 21
- 22 [70] O'Leary, D.M., Ruth, A.A., Dixneuf, S., Orphal, J., Varma, R.: The near infrared cavity-enhanced absorption spectrum of methylcyanide. *J. Quant. Spectrosc. Radiat. Transf.* **113**, 1138-1147 (2012)
- 23
- 24
- 25 [71] Czyżewski, A., Chudzyński, S., Ernst, K., Karasiński, G., Kilianek, Ł., Pietruczuk, A., Skubiszak, W., Stacewicz, T., Stelmaszczyk, K., Koch, B., Rairoux, P.: Cavity ring-down spectrography. *Opt. Comm.* **191**, 271-275 (2001)
- 26
- 27
- 28 [72] Scherer, J.J., Paul, J.B., Jiao, H., O'Keefe, A.: Broadband ringdown spectral photography. *Appl. Opt.* **40**, 6725-6732 (2001)
- 29
- 30 [73] Engeln, R., Meijer, G.: A Fourier transform cavity ring down spectrometer. *Rev. Sci. Instrum.* **67**, 2708-2714 (1996)
- 31
- 32 [74] Crosson, E.R., Haar, P., Marcus, G.A., Schwettman, H.A., Paldus, B.A., Spence, T.G., Zare, R.N.: Pulse-stacked cavity ring-down spectroscopy. *Rev. Sci. Instrum.* **70**, 4-10 (1999)
- 33
- 34
- 35 [75] Walsh, A., Zhao, D., Ubachs, W., Linnartz, H.: Optomechanical shutter modulated broad-band cavity-enhanced absorption spectroscopy of molecular transients of astrophysical interest. *J. Phys. Chem. A*, doi10.1021/jp310392n (2012)
- 36
- 37
- 38 [76] Neil, S.R.T., Rushworth, C.M., Vallance, C., Mackenzie, S.R.: Broadband cavity-enhanced absorption spectroscopy for real time, *in situ* spectral analysis of microfluidic droplets. *Lab Chip* **11**, 3953-3955 (2011)
- 39
- 40
- 41 [77] Johnston, P.S., Lehmann, K.K.: Cavity enhanced absorption spectroscopy using a broadband prism cavity and a supercontinuum source. *Opt. Expr.* **16**, 15013-15023 (2008)
- 42
- 43
- 44 [78] Lehmann, K.K., Johnston, P.S., Rabinowitz, P.: Brewster angle prism retroreflectors for cavity enhanced spectroscopy. *Appl. Opt.* **48**, 2966-2978 (2009)
- 45

- 1 [79] Schnippering, M., Neil, S.R.T., Mackenzie, S.R., Unwin, P.R.: Evanescent wave cavity-based spectroscopic techniques as probes of interfacial processes. *Chem. Soc. Rev.* **40**, 207-220 (2011)
- 2
3
- 4 [80] Yao, Y., Yao, J., Narasimhan, V.K., Ruan, Z., Xie, C., Fan, S., Cui, Y.: Broadband light management using low-Q whispering gallery modes in spherical nanoshells. *Nat. Commun.* **664**, doi: 10.1038/ncomms1664 (2012)
- 5
6
- 7 [81] Ashu-Ayem, E.R., Nitschke, U., Monahan, C., Chen, J., Darby, S.B., Smith, P.D., O'Dowd, C.D., Stengel, D.B., Venables, D.S.: Coastal Iodine Emissions. 1. Release of I₂ by *Laminaria digitata* in Chamber Experiments. *Environ. Sci. Technol.* **46**, 10413-10421 (2012)
- 8
9
10
- 11 [82] Langridge, J.M., Ball, S.M., Shillings, A.J.L., Jones, R.L.: A broadband absorption spectrometer using light emitting diodes for ultrasensitive, *in situ* trace gas detection. *Rev. Sci. Instrum.* **79**, 123110 (2008)
- 12
13
- 14 [83] Kennedy, O.J., et al.: An aircraft based three channel broadband cavity enhanced absorption spectrometer for simultaneous measurements of NO₃, N₂O₅ and NO₂. *Atmos. Meas. Tech.* **4**, 1759-1776 (2011)
- 15
16
- 17 [84] Fuchs, H., et al.: Intercomparison of measurements of NO₂ concentrations in the atmosphere simulation chamber SAPHIR during the NO₃Comp Campaign. *Atmos. Meas. Tech.* **3**, 21-37 (2010)
- 18
19
- 20 [85] Dorn, H.P., et al.: Intercomparison of NO₃ radical detection instruments in the atmosphere simulation chamber SAPHIR. *Atmos. Meas. Tech. Discuss.* **6**, 303-379 (2013)
- 21
- 22 [86] Monahan, C., Ashu-Ayem, E.R., Nitschke, U., Darby, S.B., Smith, P.D., Stengel, D.B., Venables, D.S., O'Dowd, C.D.: Coastal Iodine Emissions: Part 2. Chamber experiments of particle formation from *Laminaria digitata*-derived and laboratory-generated I₂. *Environ. Sci. Technol.* **46**, 10422-10428 (2012)
- 23
24
25
- 26 [87] Watt, R.S., Laurila, T., Kaminski, C.F., Hult, J.: Cavity enhanced spectroscopy of high-temperature H₂O in the near-infrared using a supercontinuum light source. *Appl. Spectrosc.* **63**, 1389-1395 (2009)
- 27
28
- 29 [88] Laurila, T., Burns, I.S., Hult, J., Miller, J.H., Kaminski, C.F.: A calibration method for broad-bandwidth cavity enhanced absorption spectroscopy performed with supercontinuum radiation. *Appl. Phys. B* **102**, 271-278 (2011)
- 30
31
- 32 [89] Axson, J.L., Washenfelder, R.A., Kahan, T.F., Young, C.J., Vaida, V., Brown, S.S.: Absolute ozone cross section in the Huggins Chappuis minimum (350-470 nm) at 296 K. *Atmos. Chem. Phys.* **11**, 11581-11590 (2011)
- 33
34
- 35 [90] Down, M.J., Tennyson, J., Orphal, J., Chelin, P., Ruth, A.A.: Analysis of an ¹⁸O and D enhanced water spectrum and new assignments for HD¹⁸O and D₂¹⁸O in the near-infrared region (6000-7000 cm⁻¹) using newly calculated variational line lists. *J. Mol. Spectrosc.* **282**, 1-8 (2012)
- 36
37
38
- 39 [91] Miller C.E., Brown, L.R.: Near infrared spectroscopy of carbon dioxide I. ¹⁶O¹²C¹⁶O line positions. *J. Mol. Spectrosc.* **228**, 329-354 (2004)
- 40
- 41 [92] Ouyang, B., Jones, R.L.: Understanding the sensitivity of cavity-enhanced absorption spectroscopy: pathlength enhancement versus noise suppression. *Appl. Phys. B* **109**, 581-591 (2012)
- 42
43

- 1 [93] Gherman, T., Kassi, S., Campargue, A., Romanini, D.: Overtone spectroscopy in the
2 blue region by cavity-enhanced absorption spectroscopy with a mode-locked femto-
3 second laser: application to acetylene. *Chem. Phys. Lett.* **383**, 353-358 (2004)
- 4 [94] Gherman, T., Romanini, D., Sagnes, I., Garnache, A., Zhang, Z.: Cavity-enhanced
5 absorption spectroscopy with a mode-locked diode-pumped vertical external-cavity
6 surface-emitting laser. *Chem. Phys. Lett.* **390**, 290-295 (2004)
- 7 [95] Morville, J., Kassi, S., Chenevier, M., Romanini, D.: Fast, low-noise, mode-by-mode,
8 cavity-enhanced absorption spectroscopy by diode-laser self-locking. *Appl. Phys. B*
9 **80**, 1027-1038 (2005)
- 10 [96] Thorpe, M.J., Moll, K.D., Jones, R.J., Safdi, B., Ye, J.: Broadband cavity ringdown
11 spectroscopy for sensitive and rapid molecular detection. *Science* **311**, 1595-1599
12 (2006)
- 13 [97] Thorpe, M.J., Adler, F., Cossel, K.C., de Miranda, M.H.G., Ye, J.: Tomography of a
14 supersonically cooled molecular jet using cavity-enhanced direct frequency comb
15 spectroscopy. *Chem. Phys. Lett.* **468**, 1-8 (2009)
- 16 [98] Cossel, K.C., Adler, F., Bertness, K.A., Thorpe, M.J., Feng, J., Raynor, M.W., Ye, J.:
17 Analysis of trace impurities in semiconductor gas via cavity-enhanced direct fre-
18 quency comb spectroscopy. *App. Phys. B-Lasers O* **100**, 917-924 (2010)
- 19 [99] Foltynowicz, A., Maslowski, P., Ban, T., Adler, F., Cossel, K.C., Briles, T.C., Ye, J.:
20 Optical frequency comb spectroscopy. *Faraday Discuss.* **150**, 23-31 (2011)
- 21 [100] Gohle, C., Stein, B., Schliesser, A., Udem, T., Hänsch, T.W.: Frequency comb
22 Vernier spectroscopy for broadband, high-resolution, high-sensitivity absorption and
23 dispersion spectra. *Phys. Rev. Lett.* **99**, 263902 (2007)
- 24 [101] Hardy, B., Raybaut, M., Dherbecourt, J.B., Melkonian, J.M., Godard, A., Mohamed,
25 A.K., Lefebvre, M.: Vernier frequency sampling: a new tuning approach in spectros-
26 copy - application to multi-wavelength integrated path DIAL. *Appl. Phys. B* **107**, 643-
27 647 (2012)
- 28 [102] Dasgupta, P.K., Rhee, J.-S.: Optical Cells with Partially Reflecting Windows as
29 Nonlinear Absorbance Amplifiers. *Anal. Chem.* **59**, 783-786 (1987)
- 30 [103] Langridge, J.M., Gustafsson, R.J., Griffiths, P.T., Cox, R.A., Lambert, R.M., Jones,
31 R.L.: Solar driven nitrous acid formation on building material surfaces containing ti-
32 tanium dioxide: A concern for air quality in urban areas? *Atmos. Environ.* **43**, 5128-
33 5131 (2009)
- 34 [104] Keabian, P.L., Robinson, W.A., Freedman, A.: Optical extinction monitor using CW
35 cavity enhanced detection. *Rev. Sci. Instrum.* **78**, 063102 (2007)
- 36 [105] Biennier, L., Salama, F., Gupta, M., O'Keefe, A.: Multiplex integrated cavity output
37 spectroscopy of cold PAH cations. *Chem. Phys. Lett.* **387**, 287-294 (2004)
- 38 [106] Czyżewski, A., Ernst, K., Karasinski, G., Lange, H., Rairoux, P., Skubiszak, W.,
39 Stacewicz, T.: Cavity ring-down spectroscopy for trace gas analysis. *Acta Phys. Pol.*
40 **B 33**, 2255-2265 (2002)
- 41 [107] Shillings, A.J.L., Ball, S.M., Barber, M.J., Tennyson, J., Jones, R.L.: An upper limit
42 for water dimer absorption in the 750 nm spectral region and a revised water line list.
43 *Atmos. Chem. Phys.* **11**, 4273-4287 (2011)